Stable carbon isotope patterns of marine biomarker lipids in the Arctic Ocean during Eocene Thermal Maximum 2

Petra L. Schoon,[1] Appy Sluijs,[2] Jaap S. Sinninghe Damsté,[1,3] and Stefan Schouten[1,3]

Received 13 July 2010; revised 12 May 2011; accepted 24 May 2011; published 25 August 2011.

[1] The middle Paleocene through early Eocene long-term gradual warming was superimposed by several transient warming events, such as the Paleocene-Eocene Thermal Maximum (PETM) and Eocene Thermal Maximum 2 (ETM2). Both events show evidence for extreme global warming associated with a major injection of carbon into the ocean-atmosphere system, but the mechanisms of carbon injection and many aspects of the environmental response are still poorly understood. In this study, we analyzed the concentration and stable carbon isotopic ($\delta^{13}C$) composition of several sulfur-bound biomarkers derived from marine photoautotrophs, deposited in the Arctic Ocean at ~85°N, during ETM2. The presence of sulfur-bound biomarkers across this event points toward high primary productivity and anoxic bottom water conditions. The previously reported presence of isorenieratene derivatives indicates euxinic conditions in the photic zone, likely caused by a combination of enhanced primary productivity and salinity stratification. The negative carbon isotope excursion measured at the onset of ETM2 for several biomarkers, ranges between 3‰ and 4.5‰, much larger than the ~1.4‰ recorded in marine carbonates elsewhere, suggesting substantial enhanced isotopic fractionation by the primary producers likely due to a significant rise in pCO_2. In the absence of biogenic carbonates in the ETM2 section of our core we use coeval planktonic $\delta^{13}C$ from elsewhere to estimate surface water $\delta^{13}C$ in the Arctic Ocean and then apply the relation between isotopic fractionation and pCO_2, originally calibrated for haptophyte alkenones, to three selected organic biomarkers (i.e., S-bound phytane, C_{35} hopane, and a C_{25} highly branched isoprenoid). This yields pCO_2 values potentially in the range of four times preindustrial levels. However, these estimates are uncertain because of a lack of knowledge on the importance of pCO_2 on photosynthetic isotopic fractionation.

Citation: Schoon, P. L., A. Sluijs, J. S. Sinninghe Damsté, and S. Schouten (2011), Stable carbon isotope patterns of marine biomarker lipids in the Arctic Ocean during Eocene Thermal Maximum 2, *Paleoceanography*, *26*, PA3215, doi:10.1029/2010PA002028.

1. Introduction

[2] One of the most prominent features of Cenozoic climate is a global warming trend that started in the mid-Paleocene (~59 Ma) and culminated during the Early Eocene Climatic Optimum (EECO; 52–50 Ma). During this time, several transient and geologically rapid episodes of extreme warming, or 'hyperthermals', occurred [e.g., *Zachos et al.*, 2008; *Lourens et al.*, 2005]. These hyperthermals are characterized by a pronounced negative carbon isotope excursion (CIE) recorded in both organic and inorganic carbon reservoirs, and widespread, though variable, dissolution of deep sea carbonates [*Lourens et al.*, 2005; *Sluijs et al.*, 2007; *Stap et al.*, 2010; *Leon-Rodriguez and Dickens*, 2010]. These negative CIEs are generally thought to reflect the release of large amounts of ^{13}C-depleted carbon into the exogenic carbon pool [*Dickens*, 2003]. The extensively studied Paleocene-Eocene Thermal Maximum (PETM, ~56 Ma), was further characterized by ~4–9°C warming of the continents and deep and surface ocean waters [e.g., *Kennett and Stott*, 1991; *Tripati and Elderfield*, 2005; *Wing et al.*, 2005; *Sluijs et al.*, 2006; *Weijers et al.*, 2007]. Approximately two million years later, the PETM was followed by Eocene Thermal Maximum 2 (ETM2) and the H2 hyperthermal events, characterized by similar climatic and geochemical changes as the PETM but of smaller magnitude [*Lourens et al.*, 2005; *Nicolo et al.*, 2007; *Sluijs et al.*, 2009; *Stap et al.*, 2009, 2010].

[3] Critically, the magnitude of the CIE of the global exogenic carbon pool across the PETM remains contentious [*Dickens*, 2011]. Generally, calcium carbonate precipitated by benthic foraminifera in the deep ocean or outer shelf are

[1]Department of Marine Organic Biogeochemistry, NIOZ Royal Netherlands Institute for Sea Research, Den Burg, Netherlands.
[2]Biomarine Sciences, Laboratory of Palaeobotany and Palynology, Institute of Environmental Biology, Faculty of Science, Utrecht University, Utrecht, Netherlands.
[3]Department of Earth Sciences–Geochemistry, Faculty of Geosciences, Utrecht University, Utrecht, Netherlands.

0883-8305/11/2010PA002028

considered to reliably reflect the global average magnitude of the CIE. However, the magnitude of the CIE may differ by up to 2‰ between such records [e.g., *John et al.*, 2008; *McCarren et al.*, 2008]. In part, this likely reflects regional or local climate-driven deviations in the stable carbon isotopic composition ($\delta^{13}C$) of dissolved inorganic carbon from mean ocean values, which may regionally increase or decrease the magnitude of the CIE. In addition, part of the marine CIE signal may regionally be truncated in the deep sea due to severe dissolution and temporal absence of the critical foraminifera species during the early stages of the event [e.g., *Thomas et al.*, 2002; *McCarren et al.*, 2008]. Finally, the magnitude of the CIE as recorded in foraminifera may have been dampened due to a decrease in seawater pH [*Uchikawa and Zeebe*, 2010]. The terrestrial CIE signal as recorded in paleosol carbonates is on average ~1–2‰ larger than the marine signal [*Bowen et al.*, 2001]. Although, in theory, the terrestrial carbonates should record the atmospheric CIE more directly, they may have been affected by diagenesis, and increased relative humidity and soil moisture [e.g., *Bowen et al.*, 2004]. A large (4.5‰) CIE was also recorded in organic dinoflagellate cysts in two marginal marine sections [*Sluijs et al.*, 2007], but, as yet, it remains uncertain if local factors other than the stable carbon isotopic composition ($\delta^{13}C$) of dissolved inorganic carbon influenced these records. Recent studies based on higher plant leaf wax *n*-alkanes [*Handley et al.*, 2008; *Pagani et al.*, 2006b; *Smith et al.*, 2007] suggest a large magnitude of the PETM-CIE. However, biomarker analysis showed that angiosperms and gymnosperms have a different response to the environmental changes that took place during the PETM, resulting in different isotopic fractionation, causing an overestimation of the CIE [*Schouten et al.*, 2007]. The large CIE signal of ~6‰ generally recorded in terrestrial *n*-alkanes can therefore be explained by a shift in vegetation patterns from gymnosperm dominated to angiosperm dominated [*Schouten et al.*, 2007; *Smith et al.*, 2007]. Indeed, a recent tropical *n*-alkane record that should not be affected by such biases suggests a magnitude closer to 3‰ [*Jaramillo et al.*, 2010].

[4] Molecular isotopic investigations on aquatic biomarkers have been limited to the $\delta^{13}C$ record of the C_{17} *n*-alkanes, possibly derived from algae and photosynthetic bacteria, which showed a lower CIE (~3.5‰) compared to that of the terrestrial *n*-alkanes (5–6‰) [*Pagani et al.*, 2006b]. However, it was suggested that the CIE recorded in the *n*-C_{17} alkanes was affected by increased paleoproductivity [*Pagani et al.*, 2006b]. The isotopic response of marine primary producers during the PETM remains, therefore, poorly constrained.

[5] In contrast to the PETM, $\delta^{13}C$ records of the CIE across ETM2 are relatively sparse [*Lourens et al.*, 2005; *Nicolo et al.*, 2007; *Sluijs et al.*, 2009; *Stap et al.*, 2010; *Leon-Rodriguez and Dickens*, 2010]. At Walvis Ridge, the magnitudes of warming (~3°C), carbonate dissolution and the CIE in benthic foraminifera (~1.4‰) are smaller than those at the PETM [*Lourens et al.*, 2005; *Stap et al.*, 2009, 2010]. ETM2 has recently been recognized in sediments deposited in the Central Arctic Ocean [*Sluijs et al.*, 2009; *Stein et al.*, 2006]. In a recent study, *Sluijs et al.* [2009] found cysts of freshwater tolerant dinoflagellate species to dominate assemblages during ETM2, suggesting a freshening, stratification, and eutrophication of the Arctic Ocean surface waters. Bottom water anoxia was inferred from the presence of laminated sediments and the absence of organic linings of benthic foraminifera [*Sluijs et al.*, 2009]. Furthermore, at some occasions anoxic conditions even reached into the photic zone, based on the presence of isorenieratene derivatives. The sea surface temperature proxy TEX'_{86} [*Sluijs et al.*, 2006] indicated that Arctic Ocean surface waters warmed by ~4°C during ETM2 [*Sluijs et al.*, 2009] though these estimates have some uncertainties (see detailed discussion in the Supplementary of *Sluijs et al.* [2009]). In addition, the presence of palm pollen in the interval of peak warmth implies that the mean temperature of the coldest month was above 8°C, constraining the lower temperature limit of the Arctic region during this Eocene hyperthermal event. This minimum temperature estimate is inferred from the habitats of modern biota. Paleobotanical inspection suggests that the stem structures of Paleogene palms is very similar to modern relatives which renders it highly unlikely that the palms were more resilient than at present [e.g., *Royer et al.*, 2002; *Greenwood and Wing*, 1995]. The CIE in total organic carbon (TOC) is ~3.5‰, [*Sluijs et al.*, 2009], much larger than recorded in carbonates deposited elsewhere [*Cramer et al.*, 2003; *Lourens et al.*, 2005; *Nicolo et al.*, 2007; *Stap et al.*, 2009]. However, this bulk organic carbon isotope record may have been biased due to changes in the source (i.e., terrestrial versus marine) of the bulk organic carbon.

[6] To investigate the response of marine organisms across ETM2, we analyzed the concentrations and carbon isotopic composition of sulfur-bound biomarkers derived from marine phytoplankton in the Arctic Ocean record. Furthermore, we made a first attempt to roughly estimate changes in pCO_2 across ETM2, using reconstructed carbon isotope fractionations of three independent groups of marine microorganisms. Such pCO_2 estimates would considerably improve the insight in feedback mechanisms and climate sensitivity during past episodes of abrupt warming.

2. Methods and Materials

2.1. Sample and Site Description

[7] In 2004, Integrated Ocean Drilling Program (IODP) Expedition 302, also known as the Arctic Coring Expedition (ACEX), recovered lengthy portions of a 428 m marginal marine sedimentary sequence, at the crest of the Lomonosov Ridge in the Central Arctic Ocean (~85°N paleolatitude) (Figure 1) [*O'Regan et al.*, 2008]. Uppermost Paleocene and lower Eocene sediments deposited between 56 and 50 Ma consist of siliciclastic mudstones, barren of siliceous and calcium carbonate microfossils, but containing ample immature organic matter with a TOC content of up to 8% [*Stein et al.*, 2006; *O'Regan et al.*, 2008]. As suggested by the regular occurrence of dark laminated silty clays [*O'Regan et al.*, 2008], the high content of total sulfur [*Ogawa et al.*, 2009], the general absence of remains of benthic organisms [*O'Regan et al.*, 2008; *Sluijs et al.*, 2006, 2008], and trace metal information [*Sluijs et al.*, 2008], Arctic bottom waters were low in oxygen content throughout the studied interval covering ETM2 [*Sluijs et al.*, 2009], creating optimal conditions for biomarker preservation.

[8] We studied the sediments from before to after the carbon isotope excursion (CIE) associated with ETM2,

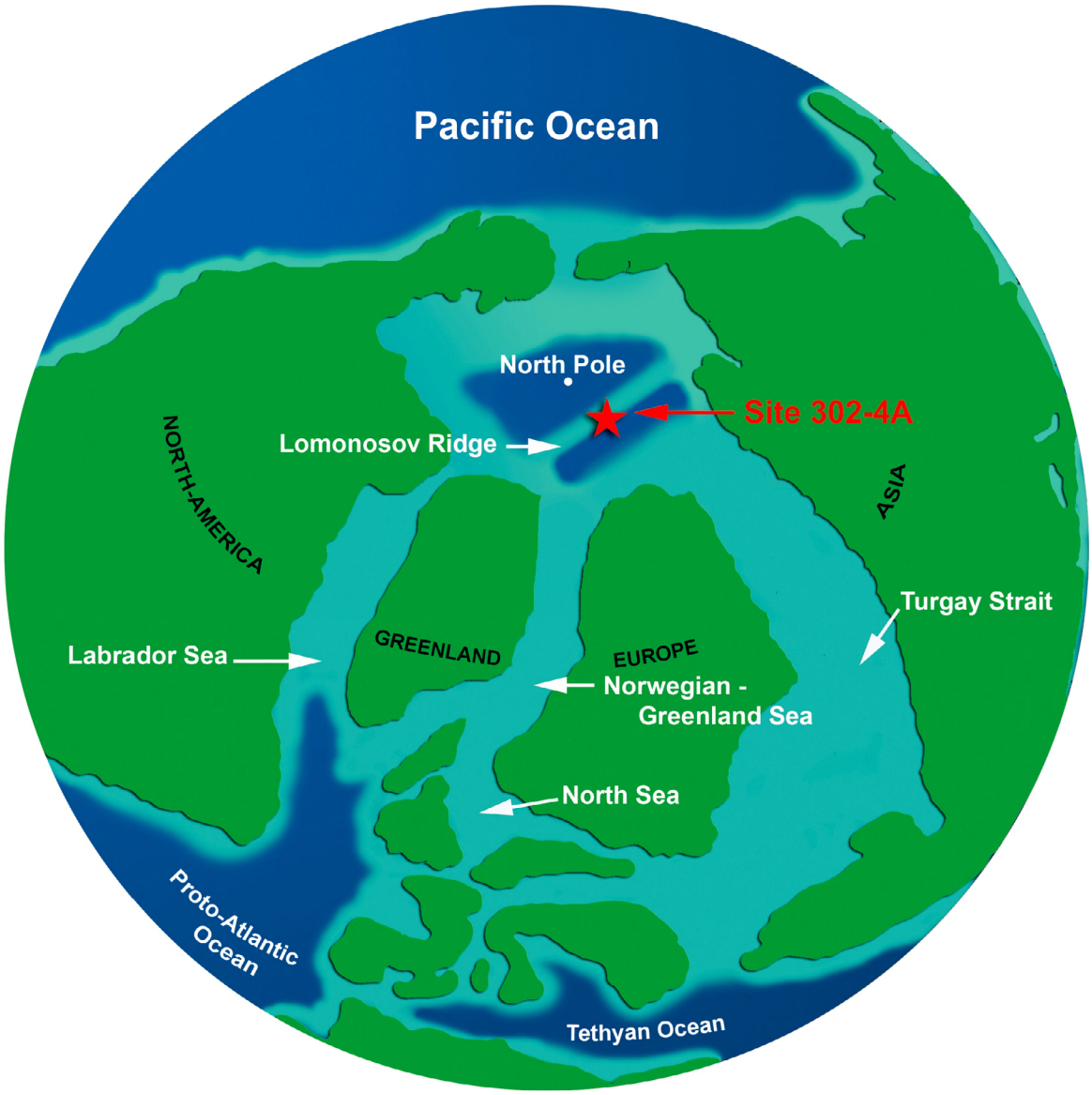

Figure 1. Paleogeographical map of the Late Paleocene–Early Eocene Central Arctic Basin showing the position of IODP Hole 302-4A (modified from *Sluijs et al.* [2009]).

which are located ~20 m above the PETM. We used the same samples of *Sluijs et al.* [2009]. The identification of the ETM2 interval is based on the presence of the dinoflagellates *Cerodinium wardenese* and *Hystrichosphaeridium tubiferum* [*Sluijs et al.*, 2008]. The onset of ETM2 is placed at ~368.9 m composite depth below seafloor (mcd) according to the $\delta^{13}C$ composition of TOC [*Sluijs et al.*, 2009].

2.2. Biomarker Analysis

[9] Powdered and freeze-dried sediments (~5 g dry mass) were extracted with a Dionex Accelerated Solvent Extractor using a 9:1 (v:v) mixture of dichloromethane (DCM) and methanol (MeOH). An aliquot of the total extract was desulfurized to release sulfur-bound hydrocarbons using Raney Nickel, as previously described by *Sinninghe Damsté et al.* [1988]. Prior to desulfurization an internal standard [2,3-dimethyl-5-(1,1-d_2-hexadecyl)thiophene] was added to the total extract aliquots for quantitative analyses. Subsequently, the desulfurized total extracts were separated into polar and apolar fractions using a small column with activated alumina using hexane/DCM (9:1;v/v) and MeOH/DCM (1:1;v/v) as eluents, respectively. The apolar desulfurized fractions containing the released hydrocarbons, were hydrogenated using PtO_2/H_2 and analyzed by gas chromatography (GC) and GC/mass spectrometry (MS). GC analyses were performed using a Hewlett-Packard 6890 instrument equipped with a flame ionization detector (FID), a Flame Photometric Detector (FPD), and an on-column injector. A fused silica capillary column (25 m × 0.32 mm) coated with CP-Sil 5 (film thickness 0.12 μm) was used with helium as carrier gas. The oven was programmed at a starting (injection) temperature of 70°C, which rose to 130°C at 20°C/min and then to 320°C at 4°C/min, at which it was maintained for 20 min. GC/MS analysis was

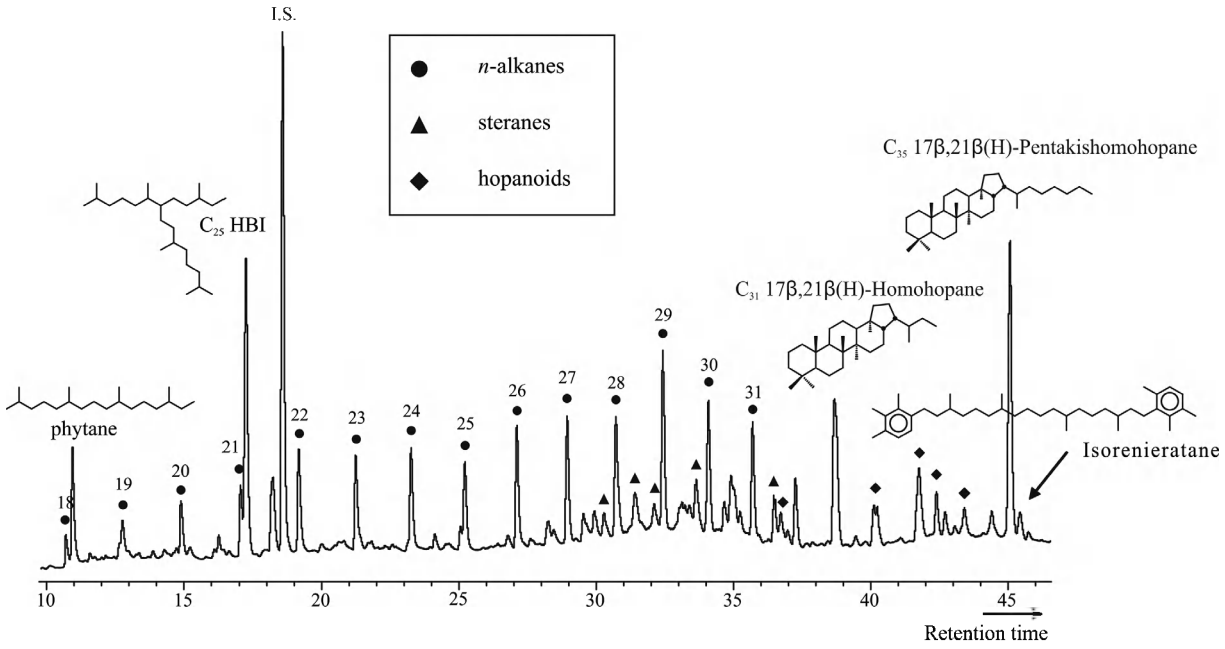

Figure 2. GC chromatogram of the desulfurized apolar fraction of sample 302-4A-27X-1, 118–120. Indicated are the *n*-alkanes (circles), C_{27}–C_{29} steranes (triangles), and C_{30}–C_{35} hopanes (diamonds). Chemical structures of the S-bound biomarkers of which the concentrations and $\delta^{13}C$ values were measured are indicated at the corresponding peaks.

done using a Thermofinnigan TRACE gas chromatograph using similar GC conditions as described above. The gas chromatograph was coupled with a Thermofinnigan DSQ quadrupole mass spectrometer with ionization energy of 70 eV and fractions were analyzed in full scan mode with a mass range of m/z 50–800 at three scans per second.

[10] To prevent coelution, *n*-alkanes were removed from the apolar fraction using a small column containing silicalite and cyclohexane as eluent [*West et al.*, 1990], before biomarker $\delta^{13}C$ analyses. The samples were analyzed on a Finnigan Delta V isotope ratio monitoring mass spectrometer coupled to an Agilent 6890 GC. Samples, dissolved in *n*-hexane, were analyzed using GC under conditions as described above. All carbon isotope compositions for the individual components are reported relative to the Vienna Pee Dee Belemnite (VDPB) standard and are average values of at least two runs.

3. Results

3.1. Biomarker COMPOSITION

[11] Analysis of selected apolar fractions of sediments in the studied ETM2 interval showed a relatively high abundance of organic sulfur compounds (OSCs), such as C_{25} HBI thiolanes [*Kohnen et al.*, 1990] and a C_{35} hopanoid thiophene [*Valisolalao et al.*, 1984]. The presence of these low molecular weight organic sulfur compounds suggests that sulfur has reacted with functionalized labile lipids and likely indicates the presence of more complex, higher molecular weight, organic sulfur compounds [*Sinninghe Damsté and de Leeuw*, 1990], which can potentially bias the distribution of biomarkers in apolar fractions [*Kohnen et al.*, 1991]. Therefore, to release all S-bound carbon skeletons we desulfurized the total extracts using Raney Nickel [*Sinninghe Damsté et al.*, 1988]. Apolar fractions of the desulfurized extracts contain mostly S-bound hydrocarbons, including 5α-C_{27}–C_{29} steranes, C_{30}–C_{35} hopanes, a C_{25} HBI and isorenieratane, predominantly with the 17β,21β(H)configuration, and some free hydrocarbons, i.e., *n*-alkanes with a slight odd-over-even carbon number predominance (see Figure 2 for a typical gas chromatogram of one of the samples). We focused on five biomarkers for quantification and isotopic study (Figures 2 and 3). S-bound phytane is an early diagenetic product of S-bound phytol [*Brassell et al.*, 1986]. Whereas phytol is part of the chlorophyll *a* molecule, and consequently characteristic for all primary producers using photosynthesis, including cyanobacteria. It is unlikely that this sulfur-bound phytane derives from terrestrial chlorophyll as sulfur-incorporation occurs during early diagenesis, i.e., almost immediately after burial [e.g., *Sinninghe Damsté and de Leeuw*, 1990]. Furthermore, S-bound phytane has a different isotopic composition than that of 'free' phytane showing its different origin [*Kohnen et al.*, 1992; *Koopmans et al.*, 1999]. S-bound C_{25} HBI is derived from unsaturated C_{25} HBIs, which are synthesized by diatoms [*Volkman et al.*, 1994] and serves as a biomarker for four specific diatom genera (*Rhizosolenia*, *Haslea*, *Navicula*, and *Pleurosigma*) [*Sinninghe Damsté et al.*, 2004a, and references therein]. S-bound C_{31} 17β,21β(H)-homohopane and S-bound C_{35} 17β,21β(H)-pentakishomohopane derive from derivatives of the membrane lipid bacteriohopanepolyol. These compounds are produced by a large number of aerobic bacteria, including cyanobacteria [*Rohmer et al.*, 1992; *Talbot et al.*, 2008, and references therein], but have also been found in some strictly anaerobic bacterial groups [*Fischer*

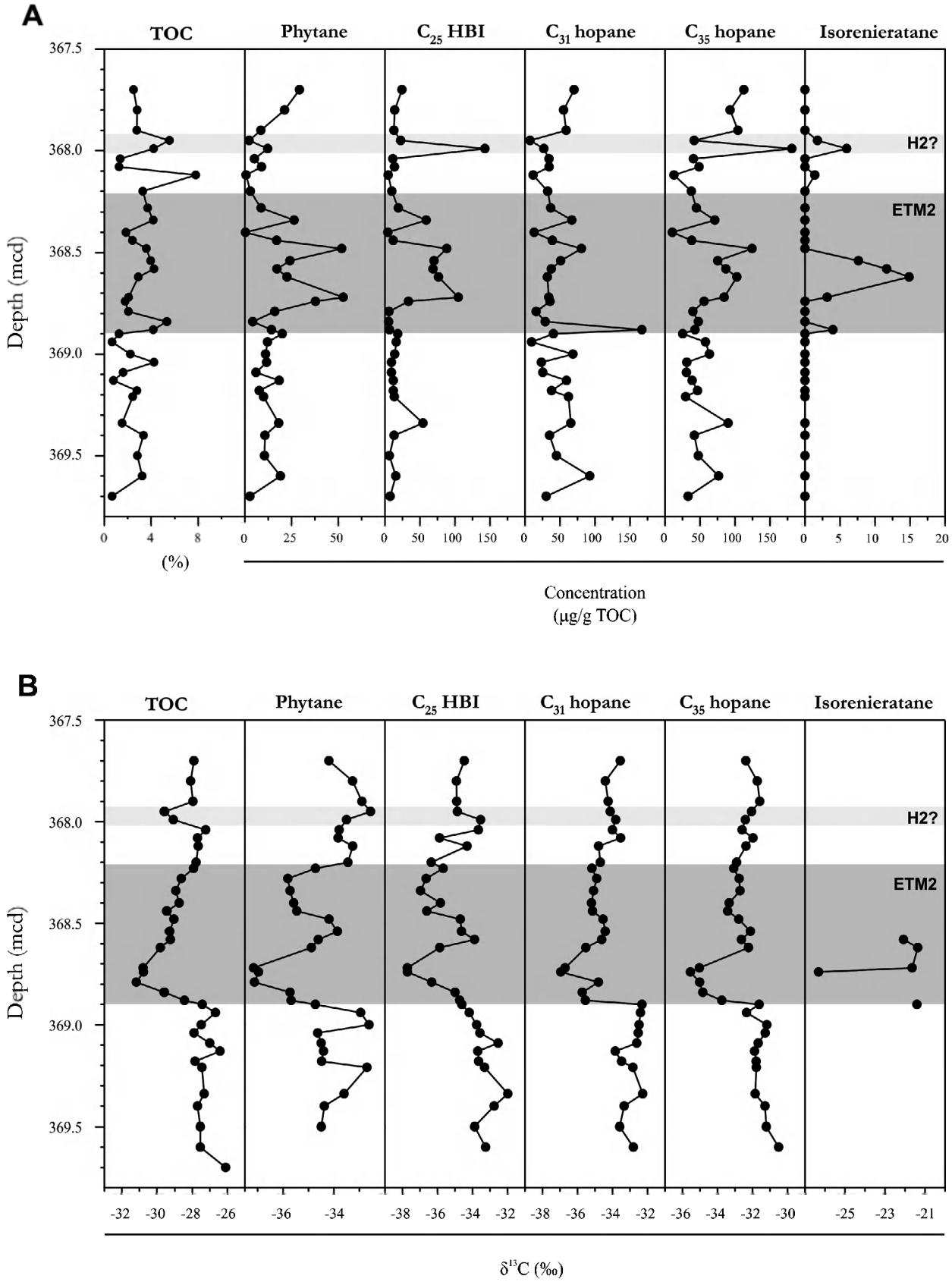

Figure 3. (a) Concentration profiles and (b) stable carbon isotope profiles of TOC [*Sluijs et al.*, 2009] and the specific S-bound biomarkers phytane, C_{25} HBI, C_{31} hopane, C_{35} hopane, and isorenieratane. The concentrations are denoted in μg/g C and $\delta^{13}C$ values are in ‰ VPDB.

Table 1. Relative Abundances of TOC and S-Bound Biomarkers

Sample	Depth (mcd)	TOC[a] (%)	Phytane	C_{25} HBI (μg/g C)	C_{31} $\beta\beta$ Hopane (μg/g C)	C_{35} $\beta\beta$ Hopane (μg/g C)	Isorenieratane (μg/g C)
302-4-27X1-30-31	367.70	2.5	29.3	24.4	70.2	112.8	n.d.
302-4-27X1-40-41	367.80	2.8	21.3	14.2	55.2	93.2	n.d.
302-4-27X1-50-51	367.90	2.8	8.6	12.8	58.9	104.2	n.d.
302-4-27X1-55-57	367.95	5.6	2.3	22.5	7.4	41.8	1.8
302-4-27X1-59-61	367.99	4.2	12.2	142.9	27.1	181.2	6.0
302-4-27X1-64-66	368.04	1.4	5.2	11.3	34.5	40.8	n.d.
302-4-27X1-68-70	368.48	1.3	9.0	13.8	34.6	48.8	n.d.
302-4-27X1-72-74	368.12	7.8	0.7	4.7	11.8	12.9	1.4
302-4-27X1-80-82	368.20	3.3	3.0	9.8	32.6	37.7	n.d.
302-4-27X1-88-90	368.28	3.7	8.7	19.3	37.0	44.8	n.d.
302-4-27X1-94-96	368.34	4.2	26.4	59.1	67.1	71.2	n.d.
302-4-27X1-100-102	368.40	1.9	0.3	4.3	13.2	10.6	n.d.
302-4-27X1-104-106	368.44	2.4	17.0	12.0	39.3	38.3	n.d.
302-4-27X1-108-110	368.48	3.6	51.9	88.4	80.8	124.4	n.d.
302-4-27X1-114-116	368.54	4.0	24.2	70.3	51.0	75.4	7.6
302-4-27X1-118-120	368.58	4.3	17.2	68.7	37.8	87.1	11.7
302-4-27X1-122-124	368.62	2.9	22.6	76.5	32.1	102.8	14.9
302-4-27X1-132-134	368.72	2.1	52.7	104.9	34.2	84.5	3.2
302-4-27X1-134-136	368.74	1.8	37.8	33.8	35.8	56.0	n.d.
302-4-27X1-139-141	368.79	2.1	16.0	5.9	16.0	39.9	n.d.
302-4-27X1-144-146	368.84	5.3	4.2	5.5	29.1	47.7	n.d.
302-4-27X1-148-150	368.88	4.2	14.3	6.6	167.0	42.9	4.0
302-4-27X2-0-2	338.90	1.3	20.1	18.4	40.7	25.3	n.d.
302-4-27X2-4-6	368.94	0.7	12.2	16.2	9.5	58.0	n.d.
302-4-27X2-12-14	369.00	2.2	11.1	14.1	68.6	63.5	n.d.
302-4-27X2-14-16	369.04	4.3	11.7	9.5	23.5	31.3	n.d.
302-4-27X2-19-21	369.09	1.6	6.0	9.4	25.6	30.7	n.d.
302-4-27X2-23-25	369.13	0.8	18.4	12.1	59.5	38.9	n.d.
302-4-27X2-28-30	369.18	2.8	7.7	12.0	38.0	46.7	n.d.
302-4-27X2-31-33	369.21	2.4	10.0	13.6	62.3	29.6	n.d.
302-4-27X2-44-45	369.34	1.5	18.1	54.4	65.6	90.3	n.d.
302-4-27X2-50-51	369.40	3.4	10.8	13.3	35.2	42.0	n.d.
302-4-27X2-60-61	369.50	2.8	10.6	6.4	45.1	47.8	n.d.
302-4-27X2-70-72	369.60	3.2	19.1	15.5	92.6	76.7	n.d.
302-4-27X2-80-81	369.70	0.7	2.7	7.5	30.3	33.0	n.d.

[a]Previously published by *Sluijs et al.* [2009].

et al., 2005; *Sinninghe Damsté et al.*, 2004b]. The source of these compounds is therefore uncertain. We did not detect any 2-methyl hopanoids, which are considered to be specific for most, although not all, cyanobacteria [*Summons et al.*, 1999] and therefore a cyanobacterial origin for S-bound C_{35} hopane cannot be confirmed. However, it is often presumed, based on isotopic studies, that C_{35} hopane in marine sediments is mainly derived from cyanobacteria [*Schoell et al.*, 1994; *Sinninghe Damsté et al.*, 2008]. Previously, we reported the presence of low amounts of S-bound isorenieratane in sediments between 368.9 and 367.9 mcd [*Sluijs et al.*, 2009]. The precursor of S-bound isorenieratane is the diaromatic carotenoid isorenieratene. This pigment is produced by the brown strain of green sulfur bacteria, which are anaerobic photoautotrophs that thrive under euxinic (high free sulfide and low oxygen) conditions within the photic zone [*Sinninghe Damsté et al.*, 1993]. In summary, it is likely that the selected biomarkers, except for S-bound isorenieratane, are all derived from marine primary producers, particularly as they are sulfur-bound and thus derived from labile precursors. Hence, they can provide insight into the response of these groups of organisms during ETM2 in the Arctic Ocean.

3.2. Biomarker Abundance

[12] In the interval just below the CIE, concentrations of phytane and C_{25} HBI, both indicators for marine phytoplankton, are low (<15 μg/g TOC; Table 1 and Figure 3a). In contrast, both bacterial biomarkers, the C_{31} and C_{35} hopane, are relatively abundant (>45 μg/g TOC), while isorenieratane is below detection limit. Across the onset of the CIE, all biomarker concentrations remain relatively low, except for a short-lived increase in C_{31} hopane concentrations (up to ~170 μg/g TOC) at ~368.88 mcd. This coincides with the first detection of isorenieratane (~4 μg/g TOC). Immediately after the peak of the CIE, at ~368.72 mcd, phytane, C_{35} hopane and the C_{25} HBI concentrations sharply increase, with peak values of ~50, ~100, and ~120 μg/g TOC, respectively. Isorenieratane is detected between 368.74 and 368.48 mcd, with peak concentrations of ~15 μg/g C at 368.62 mcd [*Sluijs et al.*, 2009]. Concentrations of phytane, the C_{25} HBI and C_{35} hopane are relatively high during this interval, but are relatively low at ~368.62 mcd where the isorenieratane concentration reaches its maximum. The C_{31} hopane abundance remains relatively constant across the interval of detectable isorenieratane. Above 368.48 mcd, all biomarker concentrations return toward the "background" pre-ETM2 values. However, elevated isorenieratane, C_{25} HBI and C_{35} hopane concentrations reoccur between 367.99 and 367.90 mcd. This interval also exhibits a negative excursion in $\delta^{13}C_{TOC}$ (Figure 3b) and was therefore suggested by *Sluijs et al.* [2009] as a potential candidate for the H2 event [*Cramer et al.*, 2003], which has recently been shown to also reflect a hyperthermal [*Stap et al.*, 2010].

Table 2. Stable Carbon Isotopic Composition (in ‰ VPDB) and Standard Deviation of TOC and S-Bound Biomarkers[a]

Sample	Depth (mcd)	$\delta^{13}C$ (‰)					
		TOC	Phytane	C_{25} HBI	C_{31} $\beta\beta$ Hopane	C_{35} $\beta\beta$ Hopane	Isorenieratane
302-4-27X1-30-31	367.70	−27.9	−34.2	−34.5	−33.5	−32.4	
302-4-27X1-40-41	367.80	−28.1	−33.3 ± 0.1	−34.9 ± 0.0	−34.4 ± 0.2	−31.7 ± 0.1	
302-4-27X1-50-51	367.90	−28.0	−32.9	−34.9	−34.2 ± 0.5	−31.6 ± 0.2	
302-4-27X1-55-57	367.95	−29.6	−32.6 ± 0.1	−34.9 ± 0.2	−34.1 ± 0.3	−32.0 ± 0.6	
302-4-27X1-59-61	367.99	−29.1	−33.5 ± 0.1	−33.5 ± 0.1	−33.8 ± 0.4	−32.4 ± 0.3	
302-4-27X1-64-66	368.04	−27.2	−33.8 ± 0.1	−33.7 ± 0.1	−34.0 ± 0.3	−32.6 ± 0.2	
302-4-27X1-68-70	368.08	−27.7	−33.8 ± 0.0	−35.9	−33.5 ± 0.8	−32.0 ± 0.5	
302-4-27X1-72-74	368.12	−27.7	−33.3	−34.3 ± 0.3	−34.8 ± 0.5	−32.4 ± 0.0	
302-4-27X1-80-82	368.20	−27.8	−33.4 ± 0.5	−36.3 ± 0.3	−34.7 ± 0.1	−32.9 ± 0.3	
302-4-27X1-83-85	368.23	−27.9	−34.7 ± 0.3	−35.7 ± 0.2	−35.2 ± 0.2	−33.1 ± 0.1	
302-4-27X1-88-90	368.28	−28.6	−35.8 ± 0.1	−36.6 ± 0.0	−34.9 ± 0.0	−32.8 ± 0.1	
302-4-27X1-94-96	368.34	−28.9	−35.7 ± 0.1	−37.0 ± 0.4	−35.1 ± 0.2	−32.7 ± 0.3	
302-4-27X1-100-102	368.40	−28.8	−35.6	−35.8 ± 0.0	−35.2	−33.3 ± 0.4	
302-4-27X1-104-106	368.44	−29.4	−35.5 ± 0.1	−36.6 ± 0.1	−35.1 ± 0.3	−33.4 ± 0.2	
302-4-27X1-108-110	368.48	−29.1	−34.2 ± 0.3	−34.7 ± 0.4	−34.5 ± 0.1	−32.8 ± 0.2	
302-4-27X1-114-116	368.54	−29.3	−33.9 ± 0.1	−34.6 ± 0.1	−34.4 ± 0.2	−32.1 ± 0.3	−22.1 ± 0.5
302-4-27X1-118-120	368.58	−29.3	−34.6 ± 0.1	−33.9 ± 1.2	−34.6 ± 0.3	−32.6 ± 0.3	−21.4 ± 1.2
302-4-27X1-122-124	368.62	−29.8	−34.9 ± 0.0	−35.9 ± 0.0	−35.5 ± 0.1	−32.2 ± 0.0	−21.6 ± 0.3
302-4-27X1-132-134	368.72	−30.8	−37.2 ± 0.1	−37.7 ± 0.0	−36.7 ± 0.3	−35.0 ± 0.1	−26.3
302-4-27X1-134-136	368.74	−30.8	−37.0 ± 0.1	−37.7 ± 0.1	−37.0 ± 0.3	−35.5 ± 0.2	
302-4-27X1-139-141	368.79	−31.2	−37.1 ± 0.3	−36.3 ± 0.1	−34.8 ± 0.1	−35.0 ± 0.0	
302-4-27X1-144-146	368.84	−29.6	−35.7 ± 1.0	−35.0 ± 0.6	−35.7 ± 0.3	−34.8 ± 0.3	
302-4-27X1-148-150	368.88	−28.5	−35.7 ± 0.4	−34.7 ± 0.3	−35.5 ± 0.1	−33.8 ± 0.2	−21.4 ± 0.1
302-4-27X2-0-2	368.90	−27.4	−34.7 ± 0.0	−34.6 ± 0.4	−32.3 ± 0.1	−31.6 ± 0.1	
302-4-27X2-4-6	368.94	−26.7	−33.0 ± 0.7	−34.2	−32.4	−32.3 ± 0.1	
302-4-27X2-12-14	369.00	−27.5	−32.6 ± 0.5	−33.8 ± 0.4	−32.5 ± 0.2	−31.2 ± 0.1	
302-4-27X2-14-16	369.04	−27.9	−34.6 ± 0.2	−33.7 ± 0.1	−32.5 ± 0.1	−31.3 ± 0.1	
302-4-27X2-19-21	369.09	−27.0	−34.5	−32.5	−32.6 ± 0.4	−31.7 ± 0.6	
302-4-27X2-23-25	369.13	−26.4	−34.4 ± 0.2	−33.7	−33.8 ± 0.2	−31.9 ± 0.2	
302-4-27X2-28-30	369.18	−27.8	−34.5 ± 0.8	−33.6 ± 0.5	−33.5 ± 0.3	−31.8 ± 0.1	
302-4-27X2-31-33	369.21	−27.5	−32.7 ± 0.3	−33.3 ± 0.1	−32.8 ± 0.1	−31.8 ± 0.1	
302-4-27X2-44-45	369.34	−27.3	−33.6	−32.0 ± 0.2	−32.3 ± 0.9	−31.8 ± 0.2	
302-4-27X2-50-51	369.40	−27.7	−34.4 ± 0.1	−32.8 ± 0.4	−33.3 ± 0.3	−31.3 ± 0.3	
302-4-27X2-60-61	369.50	−27.6	−34.5 ± 0.6	−33.9 ± 0.3	−33.6 ± 0.0	−31.2 ± 0.1	
302-4-27X2-70-72	369.60	−27.5		−33.2 ± 0.3	−32.8 ± 0.4	−30.5 ± 0.3	

[a]Stable carbon isotopic composition is in ‰ VPDB.

3.3. Compound-Specific Stable Carbon Isotope Analysis

[13] Stable carbon isotope analyses were performed, where possible, on phytane and C_{25} HBI as biomarkers for marine photosynthetic algae, and on C_{31} hopane and C_{35} hopane as biomarkers for (cyano)bacteria (Figure 3b and Table 2). We were able to determine the $\delta^{13}C$ composition of isorenieratane for the sediments at 368.88 and 368.72–368.54 mcd (Table 2). Isorenieratane $\delta^{13}C$ values are 11–14‰ enriched relative to phytane in the same samples. Green sulfur bacteria use the reversed tricarboxylic acid cycle that discriminates much less against ^{13}C than the Calvin cycle, which is used by most photoautotrophic organisms [*Quandt et al.*, 1977]. An enrichment of this magnitude for isorenieratane can therefore be expected and is consistent with previous observations [*Koopmans et al.*, 1996; *van der Meer et al.*, 1998].

[14] Prior to the CIE of ETM2, the carbon isotope values are relatively stable, i.e., −27.3 ± 0.6‰ for TOC, −33.9 ± 0.8‰ for phytane, −33.2 ± 0.7‰ for C_{25} HBI, −32.9 ± 0.5‰ for C_{31} hopane and −31.5 ± 0.5‰ for C_{35} hopane. The drop in $\delta^{13}C$ of the analyzed specific biomarkers is essentially synchronous with the onset of the CIE in TOC [*Sluijs et al.*, 2009], confirming the initiation of the CIE at ~368.9 mcd. This drop is ~3.2 and ~4.5‰ for the algal biomarkers phytane and C_{25} HBI respectively, and ~4.1‰ for both the C_{31} and C_{35} hopane. Except for phytane, the magnitudes of the shifts are slightly higher than the ~3.5‰ shift in TOC.

[15] Between 368.72 and 368.23 mcd, the $\delta^{13}C_{TOC}$ record shows a gradual recovery toward 'background' pre-ETM2 values. Interestingly, the biomarker $\delta^{13}C$ records show a more complex pattern (Figure 3b). An initial increase in $\delta^{13}C$ values at ~368.7 mcd, is followed by a second drop in $\delta^{13}C$ between 368.48 and 368.23 mcd for phytane and C_{25} HBI. At 368.2 mcd all biomarkers have returned to their 'background', i.e., pre-ETM2 values. The potential presence of H2, based on the $\delta^{13}C_{TOC}$ record, is not apparent in the $\delta^{13}C$ records of any of the analyzed biomarkers.

4. Discussion

4.1. Climatic and Environmental Changes Across ETM2 in the Arctic Ocean

[16] Prior to the onset of ETM2, both the biomarker concentrations and $\delta^{13}C$ values show only minor variations, suggesting that environmental conditions were relatively stable (Figures 3a and 3b). Furthermore, no isorenieratane is detected in these sediments implying that the water column was not euxinic within the photic zone. This is also supported by relatively stable assemblages of typical open marine dinoflagellate cysts in this interval [*Sluijs et al.*,

2009]. Relatively high TOC concentrations and the presence of "sulfur-bound" organic molecules in these sediments points toward a relatively productive paleoenvironment and low bottom water oxygen concentrations, which is in agreement with previous observations [*Sluijs et al.*, 2008; *Stein et al.*, 2006].

[17] The synchronous drop in $\delta^{13}C$ at ~368.9 mcd of both the specific biomarkers and TOC confirms that the CIE in TOC is not caused by changes in the composition of the bulk organic matter, but is linked to the injection of ^{13}C-depleted carbon into the global exogenic carbon pool. During the recovery of ETM2, the $\delta^{13}C$ of the biomarkers no longer track the $\delta^{13}C_{TOC}$ profile. The $\delta^{13}C_{TOC}$ record shows a smooth return to background $\delta^{13}C$ values from 368.8 mcd, while the $\delta^{13}C$ profiles of the biomarkers abruptly move toward more positive values at 368.6 mcd (Figure 3b). Additionally, directly after the CIE, at ~368.7 mcd, there is a sharp increase in concentrations of phytane, C_{25} HBI and C_{35} hopane, which is followed by the development of photic zone euxinia (PZE) as indicated by the presence of isorenieratene derivatives. Possibly, enhanced productivity contributed to the development of PZE conditions in this interval, as was suggested for ETM2 and the PETM in the Arctic Ocean [*Sluijs et al.*, 2006, 2009; *Stein et al.*, 2006]. The increase in biomarker concentrations may also be explained by an increase in export production. However, *Knies et al.* [2008] investigated the response of marine productivity to variations in nutrient supply to the Cenozoic Arctic Ocean using nitrogen isotopes. For ETM2 they found evidence for an increase in primary production rates even after correcting for the higher burial efficiency caused by the euxinic conditions. Furthermore, abundances of the freshwater tolerant dinoflagellate species that peak synchronously with isorenieratane concentrations are also regarded as indicators for nutrient-rich conditions [*Sluijs et al.*, 2005, 2009]. Although the timing with these dinoflagellate peaks is not perfectly synchronous, an increase in primary productivity could explain the increase in biomarker concentrations and the positive isotope shift in the specific biomarkers at 368.6 mcd, as an increase in primary productivity can lead to increased growth rates and decreased isotopic fractionation [*Jasper and Hayes*, 1990; *Laws et al.*, 1995; *Bidigare et al.*, 1997; *Popp et al.*, 1998a, 1998b]. Therefore, although the lipids obviously had to be exported from the surface ocean to settle on the seafloor, the increase in concentrations in our view was at least partially related to increased productivity. This would imply that during this interval regional effects control the biomarker records, whereas TOC in this case more accurately tracks the $\delta^{13}C$ evolution of the exogenic carbon pool.

[18] At ~368.48 mcd, biomarker concentrations decrease and isorenieratane is below detection limit (Figure 3a), suggesting that the PZE conditions ended. Subsequently, all biomarker isotope values return to 'background' pre-ETM2 values and continue to track the $\delta^{13}C_{TOC}$ signal (Figure 3b).

4.2. H2 Event

[19] At ~368.0 mcd the TOC record exhibits a second negative CIE of ~2‰ (Figure 3b). This interval was previously interpreted to possibly reflect the H2 event, although a potential hiatus and the absence of a biostratigraphic framework with sufficient detail complicates exact identification [*Sluijs et al.*, 2009]. Indeed, the presence of isorenieratane coincident with the dominance of low-salinity-tolerant dinoflagellate species [*Sluijs et al.*, 2009], points to similar conditions as for ETM2. Remarkably, however, there is no negative carbon isotope shift in the biomarker $\delta^{13}C$ records. There are two possible explanations for this apparent discrepancy. (1) The negative $\delta^{13}C$ shift in TOC records an isotope excursion of the global exogenic carbon pool, but is obscured in the $\delta^{13}C$ records of the biomarkers because of an increase in productivity, although this likely should have affected $\delta^{13}C_{TOC}$ as well. (2) The shift in the $\delta^{13}C_{TOC}$ record is not recording a CIE but is caused by a change in source material transported toward the Arctic Basin. None of these explanations can be completely excluded and, thus, the nature of this interval cannot be further elucidated based on the $\delta^{13}C$ profiles of these marine biomarkers.

4.3. Estimating Isotopic Fractionation Across ETM2

[20] Based on the measured stable isotopic composition of S-bound phytane, C_{25}HBI and C_{35} hopane, we estimated the average carbon isotopic fractionation of photoautotrophs, and changes therein. Averaged $\delta^{13}C$ values were calculated for three time intervals: the pre-ETM2 interval (369.60–368.94 mcd), the CIE of ETM2 (368.84–368.72 mcd), and the post-ETM2 interval (368.20–368.04 mcd). Average biomarker $\delta^{13}C$ values for these three periods were used to estimate the isotopic fractionation (ε_p):

$$\varepsilon_p = 10^3\left[(\delta_d + 1000)/(\delta_p + 1000) - 1\right], \quad (1)$$

where δ_p is the $\delta^{13}C$ value of the total organic carbon of the organism and δ_d is the $\delta^{13}C$ value of the carbon substrate. To obtain δ_p, a correction must be made for the isotopic offset between the biomarker lipid and cell biomass. *Schouten et al.* [1998] and *Oakes et al.* [2005] reported, based on culture experiments and literature study of a range of different algae, that phytol is ~6‰ depleted relative to the total algal biomass. For C_{25} HBIs a depletion of 6.6‰ relative to biomass was reported by *Schouten et al.* [1998] for the diatom *Rhizosolenia setigera*, whereas *Massé et al.* [2004] found similar carbon isotopic compositions of the C_{25} HBIs and phytol in *Haslea ostrearia*. This suggests an isotopic offset of ca. 6‰ for both phytane and C_{25} HBI. Results from culture experiments of the cyanobacterium species *Synechocystis* revealed an isotopic offset of 8.4‰ for bishomohopanol [*Sakata et al.*, 1997].

[21] Values for δ_d can be obtained from the carbonate shells of planktonic foraminifera using the following equation:

$$\delta_d \approx \delta^{13}C_{pf} - 1 + (24.12 - 9866/T). \quad (2)$$

The $\delta^{13}C$ of planktonic foraminifera ($\delta^{13}C_{pf}$) represents the $\delta^{13}C$ composition of the primary carbon in $CaCO_3$. The term between brackets describes the isotopic effect associated with the equilibrium exchange reaction between CO_{2aq} and HCO_3^- as reported by *Mook et al.* [1974], which only depends on temperature (T in degrees Kelvin).

[22] Unfortunately, foraminiferal carbonate is absent in ACEX sediments [*Sluijs et al.*, 2008, 2009]. Instead, we used the $\delta^{13}C$ values of the surface-dwelling genus *Acarinina* reported for ETM2 at Walvis Ridge [*Lourens et al.*,

Table 3. Estimations for pCO_2 Based on the $\delta^{13}C$ Composition of S-Bound Phytane, C_{25} HBI, and C_{35} Hopane

Biomarker	$\delta^{13}C$[a] (‰)	$\Delta\delta$[b] (‰)	δ_p[c] (‰)	$\delta^{13}C_{pf}$[d] (‰)	SST-WR[e] (°C)	SST-AO[f] (°C)	δ_d[g] (‰)	ε_p[h] (‰)	ε_f[i] (‰)	K_0[j] (mol L^{-1} atm^{-1})	pCO_2[k] (ppmv) b = 160	b = 200	b = 240
Preexcursion Interval (369.60–368.94 mcd)													
S-bound phytane	−33.9 ± 0.4	6	−27.9	2	18.5	19	−8.7	19.7	25	0.03431	900	1100	1300
S-bound phytane	−33.9 ± 0.4	6	−27.9	2	18.5	19	−8.7	19.7	27	0.03431	650	800	950
S-bound HBI	−33.3 ± 0.3	6	−27.3	2	18.5	19	−8.7	19.1	25	0.03431	800	1000	1200
S-bound HBI	−33.3 ± 0.3	6	−27.3	2	18.5	19	−8.7	19.1	27	0.03431	600	750	900
S-bound C_{35} hopane	−31.5 ± 0.2	8.4	−23.1	2	18.5	19	−8.7	14.7	20	0.03431	900	1100	1350
Excursion Interval (368.84–368-72 mcd)													
S-bound phytane	−36.7 ± 0.4	6	−30.7	0	21.5	23	−10.4	21.0	25	0.0307	1300	1650	1950
S-bound phytane	−36.7 ± 0.4	6	−30.7	0	21.5	23	−10.4	21.0	27	0.0307	850	1100	1300
S-bound HBI	−36.7 ± 0.2	6	−30.7	0	21.5	23	−10.4	20.9	25	0.0307	1300	1600	1900
S-bound HBI	−36.7 ± 0.2	6	−30.7	0	21.5	23	−10.4	20.9	27	0.0307	850	1100	1300
S-bound C_{35} hopane	−35.1 ± 0.2	8.4	−26.7	0	21.5	23	−10.4	16.8	20	0.0307	1600	2000	2400
Postexcursion Interval (368.20–368.04 mcd)													
S-bound phytane	−33.6 ± 0.2	6	−27.6	1.5	17.5	18	−9.3	18.8	25	0.0353	750	900	1100
S-bound phytane	−33.6 ± 0.2	6	−27.6	1.5	17.5	18	−9.3	18.8	27	0.0353	550	700	850
S-bound HBI	−33.1 ± 0.2	6	−27.1	1.5	17.5	18	−9.3	18.2	25	0.0353	650	850	1000
S-bound HBI	−33.1 ± 0.2	6	−27.1	1.5	17.5	18	−9.3	18.2	27	0.0353	500	650	800
S-bound C_{35} hopane	−32.5 ± 0.3	8.4	−24.1	1.5	17.5	18	−9.3	15.1	20	0.0353	900	1150	1400

[a]The average $\delta^{13}C$ compositions of the indicated biomarkers.
[b]The isotopic offset between lipids and biomass for algae [*Schouten et al.*, 1998; *Massé et al.*, 2004; *Oakes et al.*, 2005] and for cyanobacteria [*Sakata et al.*, 1997].
[c]Estimated stable carbon isotopic composition of the primary photosynthate calculated from the $\delta^{13}C$ composition of the biomarkers and $\Delta\delta$.
[d]Average $\delta^{13}C$ of inorganic carbonate of the planktonic foraminifer *A. soldadoensis* measured in sediments of Sites 1263, 1265, and 1267 at Walvis Ridge [*Lourens et al.*, 2005; *Stap et al.*, 2010].
[e]Average sea surface temperatures for Walvis Ridge obtained from the $\delta^{18}O$ [*Stap et al.*, 2010].
[f]Average sea surface temperatures obtained from TEX'_{86} [*Sluijs et al.*, 2009] for the ACEX sediments at Arctic Ocean.
[g]The carbon isotopic composition of $CO_{2(aq)}$.
[h]The calculated isotopic fractionation associated with the photosynthetic fixation of carbon.
[i]The maximum isotopic fractionation associated with the photosynthetic fixation of carbon.
[j]The solubility constant K_0 of Henry's Law from *Weiss* [1974].
[k]The calculated atmospheric CO_2 concentration for three different *b* values.

2005; *Stap et al.*, 2010]. Although this induces one factor of uncertainty, the $\delta^{13}C_{pf}$ of ~2‰ for the period prior to ETM2 compares quite well with those of stacked carbonate isotope records, as well as with modeling studies for the Early Eocene [*Hayes*, 1999; *Berner*, 2006; *Berner and Kothavala*, 2001], suggesting that this assumption is reasonable. We do not believe that in the semi-enclosed Arctic Basin additional effects, such as the input of recycled CO_2 from anoxic deep waters play a large role. *Van Breugel et al.* [2006] demonstrated that in an anoxic marine system the effect of recycling of respired CO_2 on the $\delta^{13}C$ of phytoplankton lipids is negligible. Sea surface temperatures (SSTs) used in equation (2) were obtained from the oxygen isotopes of the same foraminiferal records from Walvis Ridge and a TEX_{86} measurement during ETM2 [*Stap et al.*, 2010].

[23] The calculated ε_p values for the preexcursion interval show remarkably high carbon isotope fractionation factors of ca. 21–22‰ and ca. 14.5‰ for marine algae and (cyano) bacteria, respectively (Table 3). The lower value determined for (cyano)bacteria is consistent with the smaller carbon isotopic fractionation by cyanobacteria in comparison to algae [*Hayes*, 2001; *Popp et al.*, 1998b]. During ETM2, ε_p values increase even further by 1–2‰. For all three biomarkers this results in ε_p values that lie close to the maximum fractionation of photoautotrophic organisms, i.e., 25–28‰ for the Rubisco enzyme of autotrophic eukaryotes [*Bidigare et al.*, 1997; *Goericke et al.*, 1994; *Popp et al.*, 1998b] and 16–22‰ for autotrophic cyanobacteria [*Sakata et al.*, 1997, and references therein].

[24] The magnitude of ε_p is mainly determined by the carbon fixation enzyme and carbonate concentration mechanism, which in turn can be affected by factors such as the amount of available CO_2 in the water column ($[CO_{2aq}]$), growth rate, light intensity, and species-specific factors such as cell geometry [e.g., *Jasper and Hayes*, 1990; *Laws et al.*, 1995; *Popp et al.*, 1998a, 1998b; *Cassar et al.*, 2006]. Thus, in principle, the observed increase in biomarker ε_p values during ETM2 can be caused by increased levels of $[CO_{2aq}]$, but there are several additional factors which may be potentially responsible for this. The most important ones are a decrease in specific growth rates, a change in cell geometry, a change in light intensity, and the carbon uptake mechanism [*Bidigare et al.*, 1997; *Laws et al.*, 1995; *Popp et al.*, 1998a, 1998b; *Rau et al.*, 1996; *Burkhardt et al.*, 1999]. It is unlikely that cell geometry has changed on this relative short time interval of the ETM2 for both the marine algae and (cyano)bacteria. Moreover, we also use S-bound phytane which is a biomarker not specific for only one group of organisms, but is contributed by many different species of marine algae and cyanobacteria. Furthermore, all available information indicates that productivity increased rather than decreased during ETM2 (see above), which theoretically should lead to a decrease of ε_p values. To avoid the imprint of growth rate changes on fraction-

ation, we only used $\delta^{13}C$ values before, and directly after the interval where several lines of evidence, including elevated biomarker concentrations, indicated elevated productivity (see section 4.1).

[25] Another important aspect to consider is the carbon uptake mechanism used by autotrophs during photosynthesis. Many photosynthetic organisms have evolved mechanisms to actively take up CO_2 or HCO_3^- (a so-called carbon concentrating mechanism or CCM) in order to overcome the deficiency of the enzyme Rubisco in low-CO_2/high-alkaline environments and this mechanism will impact a reduced isotopic fractionation [*Giordano et al.*, 2005]. In our case, however, the time of ETM2 most likely belonged to a high-CO_2/low-pH world, considering the large input of ^{13}C-depleted carbon, making it unlikely that they need a CCM. Furthermore, isotopic modeling which incorporates active transport shows that ε_p is still a function of growth rate and CO_2 under nutrient limitation (though this function is different under light limitation [*Cassar et al.*, 2006]). Finally, the very negative biomarker $\delta^{13}C$ values suggest that the organisms that made the lipids likely did not use a CCM, which has also been previously suggested for diatoms that biosynthesize HBI isomers [*Schouten et al.*, 2000].

[26] Growth experiments of aquatic algae indicate that light-limitation may also have a potential effect on isotopic fractionation [*Burkhardt et al.*, 1999; *Cassar et al.*, 2006]. However, at this latitude it is likely that phytoplankton thrived only during summer in full light conditions, particularly with the absence of ice at this time. The only change in light conditions could appear when the water column is more stratified and fresher during ETM2, resulting in increasing light intensity and an increase in the magnitude of isotopic fractionation. However, the time of highest stratification, i.e., when isorenieratene derivatives are present, is some time after the CIE. In contrast, this interval is marked by slightly enriched ^{13}C values for the different biomarkers. This suggests that light limitation cannot explain the isotopic fractionation patterns we observe. We, therefore, mostly attribute the increase in ε_p to a substantial increase in seawater CO_2 concentration ($[CO_{2aq}]$), in turn caused by elevated atmospheric pCO_2 levels during ETM2.

4.4. A First Attempt to Estimate pCO_2 for ETM2 Using Carbon Isotopic Fractionation Factors

[27] For alkenone-producing haptophytes the relationship between $[CO_{2aq}]$ and ε_p is relatively well constrained [*Pagani et al.*, 2002, and references therein]. Therefore, stable carbon isotopic fractionation records using long-chain alkenones are frequently used for pCO_2 reconstructions [e.g., *Andersen et al.*, 1999; *Benthien et al.*, 1999; *Pagani et al.*, 1999, 2002, 2005; *Pagani*, 2002; *Bijl et al.*, 2010; *Palmer et al.*, 2010]. However, *Popp et al.* [1998b] also reported a relation between $[CO_{2aq}]$, growth rate and cell dimension for certain diatoms and cyanobacteria, although again other factors such as light intensity may play a role as well [*Burkhardt et al.*, 1999; *Cassar et al.*, 2006]. This would imply that the carbon isotope composition of specific marine algal biomarkers, other than alkenones, may also be applicable for pCO_2 reconstructions. Indeed, ancient pCO_2 levels were determined by *Freeman and Hayes* [1992] using the carbon isotopic fractionations of sedimentary porphyrins [*Popp et al.*, 1989]. Furthermore, variations in the offset between carbonate and organic matter isotopic composition have been applied as paleo-pCO_2 proxy to reconstruct the expected drawdown in atmospheric CO_2 during the late Cenomanian oceanic anoxic event [*Jarvis et al.*, 2011]. Their trend in isotopic fractionation is remarkably consistent with previously estimated Cretaceous pCO_2 values using the $\delta^{13}C$ values of the specific marine biomarkers (S-bound) phytane and C_{35} hopane [*Bice et al.*, 2006; *Sinninghe Damsté et al.*, 2008].

[28] Here we follow the approach of *Freeman and Hayes* [1992], *Bice et al.* [2006], and *Sinninghe Damsté et al.* [2008] to provide estimates of pCO_2 during the early Eocene ETM2 interval. Large uncertainties and assumptions which are associated with this approach will be discussed below. Our goal here is merely to present estimates of the atmospheric CO_2 concentrations and changes therein, which potentially can give insight in the changes of pCO_2 levels across an Eocene hyperthermal, and provide a method which can be used at other environmental settings where similar isotopic biomarker records can be obtained.

4.4.1. Calculation of pCO_2 Estimates

[29] In order to reconstruct the atmospheric CO_2 concentrations across ETM2 from carbon isotopic fractionation factors, we assume that the relationship between ε_p and $[CO_2]_{aq}$, based on the calibration of $\delta^{13}C$ composition of alkenones, is also applicable for $\delta^{13}C$ values of other biomarkers produced by photoautotrophic organisms, in this case S-bound phytane, C_{25} HBI and C_{35} hopane. If so, then the degree of isotopic fractionation (ε_p) in a cell can in theory be related to CO_2 concentrations using the following equation [*Bidigare et al.*, 1997]:

$$\varepsilon_p = \varepsilon_f - b/[CO_{2(aq)}], \quad (3)$$

where b is the sum of species-specific factors and reflects the carbon demand of the cell. Atmospheric pCO_2 concentrations can then be estimated from the $[CO_{2(aq)}]$ values using Henry's law.

[30] For haptophyte algae it has been shown that b displays a strong positive correlation with phosphate concentrations [*Andersen et al.*, 1999; *Benthien et al.*, 2002; *Bidigare et al.*, 1997; *Pagani et al.*, 2002], and thus, if phosphate concentrations were known then b, and thereby $[CO_{2(aq)}]$, could be estimated. A similar relation, with different b values, is observed for other algae [*Popp et al.*, 1998b] and we assume here that b values of these algae also depend on nutrients such as phosphate. However, it is difficult to predict the PO_4 concentrations of Arctic surface waters, especially considering the stratified conditions during ETM2. *Andersen et al.* [1999] reported an inverse relationship between the bulk nitrogen isotopes and phosphate concentrations in equatorial and south Atlantic core top sediments. They used this relationship to reconstruct b and in turn the pCO_2 levels using their calibration of sedimentary $\delta^{13}C$ alkenones. As an approach to constrain the b value for equation (3), we applied this relationship to the Early Eocene Arctic Ocean by using the nitrogen isotope values measured by *Knies et al.* [2008], leading to average phosphate concentrations of 1.25 μmol/L prior to ETM2 to 1.5 μmol/L just at the onset of ETM2. Depending on the calibration, this leads to a b value ranging between 160 to 240. The pCO_2 estimates obtained using the approach

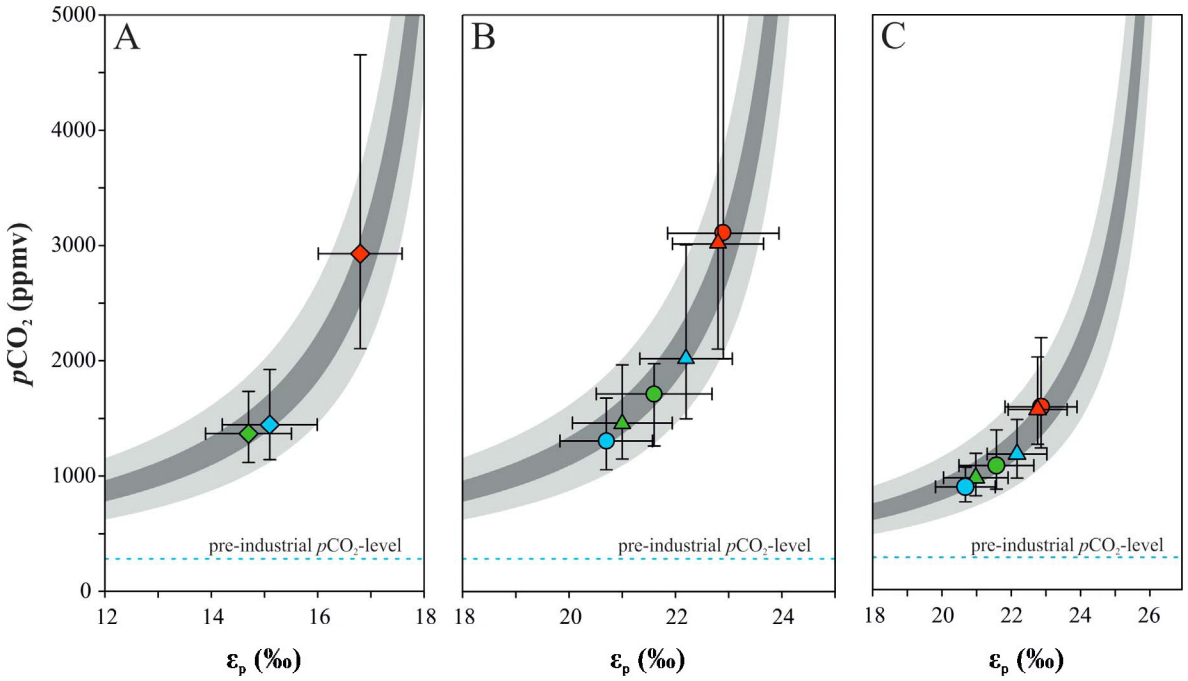

Figure 4. Estimations of the atmospheric CO_2 concentrations for the pre-ETM2 interval (green symbols), CIE of ETM2 (red symbols), and the post-ETM2 interval (blue symbols) using (a) the average $\delta^{13}C$ values of C_{35} hopane (diamonds) using a maximum fractionation level (ε_f) of 20‰, (b) the average $\delta^{13}C$ values of phytane (circles) and C_{25} HBI (triangles) with an ε_f of 25‰, and (c) the average $\delta^{13}C$ values of phytane (circles) and C_{25} HBI (triangles) using an ε_f value of 27‰. Error bars include variations in SST and $\delta^{13}C_{pf}$ of 1°C and 0.5‰, respectively, in addition to analytical errors. The gray shaded areas give the range of b (160–240) with $b = 200$ as intermediate value. Note that the uncertainty of the pCO_2 estimates increases with higher ε_p values. Minimum pCO_2 values using this approach are 590, 860, and 520 ppmv for the pre-ETM interval, the CIE of ETM2, and the post-ETM2 interval, respectively. This is at least two to three times preindustrial pCO_2 levels (blue dotted line).

outlined above are illustrated in Figure 4. Here we plotted the ε_p-CO_2 relationship of the algal biomarkers for the three time intervals at an intermediate b value of 200. The error bars include uncertainties in SST (±1°C) and $\delta^{13}C_{pf}$ (±0.5‰), in addition to the analytical errors. To illustrate the importance of b, we varied this parameter over a range of 160–240 (Table 3 and Figure 4). One has to bear in mind, though, that our pCO_2 estimates are based on the ε_p-$[CO_{2aq}]$ relationship originally calibrated for $\delta^{13}C$ alkenones [*Pagani et al.*, 2002, and references therein]. In addition, we assume that the $\delta^{13}C_{pf}$ from Walvis Ridge is a representative of that in the Arctic Ocean during the ETM2. The propagated uncertainty stemming from these assumptions is difficult to quantify and is further discussed below.

[31] For all three periods, the estimated pCO_2 values are practically similar using three independent biomarkers and all suggest that pCO_2 values were at least 2× preindustrial values, i.e., the minimum pCO_2 estimates (considering all the uncertainties). Furthermore, when using the intermediate b value, the estimated pCO_2 values are 800 to 1100 ppmv (3 to 4 times preindustrial values) for the preexcursion interval and 1100 to 2000 ppmv (4 to 7 times preindustrial values) for the CIE of ETM2 (see Table 3). Thus, pCO_2 levels during ETM2 may have been 300 to 800 ppmv higher than prior to the ETM2.

4.4.2. Uncertainties, Caveats, and Future Outlook

[32] Clearly, our estimated pCO_2 values are all associated with large uncertainties as indicated by the large error bars in Figure 4, and we caution that they should not be taken at face value. As mentioned before these pCO_2 estimates are relying on a number of assumptions: (1) the $\delta^{13}C$ composition of the DIC ($\delta^{13}C_{pf}$ in equation (2)) of the Arctic Ocean surface waters equals the surface water $\delta^{13}C$ of DIC of the subtropic SE Atlantic Ocean at Walvis Ridge during the Early Eocene; (2) the relationship between ε_p and $[CO_2]_{aq}$, based on the calibration of $\delta^{13}C$ composition of alkenones, is also applicable for $\delta^{13}C$ values of other biomarkers produced by photoautotrophic organisms, in this case S-bound phytane, C_{25} HBI and C_{35} hopane; and (3) the b value of photoautotrophs other than haptophyte algae are also related to nitrogen isotopic compositions. Since these assumptions have not yet been tested, it is not possible to estimate potential errors they introduce in the pCO_2 estimates, but clearly they will have a large impact. Furthermore, there are a number of uncertainties associated with estimations of the isotopic fractionation factors as discussed in section 4.3. For example, an uncertainty in $\delta^{13}C_{pf}$ may arise due to diagenesis and vital effects, and may be in the order of 0.5‰. An uncertainty of that magnitude will result in an equal uncertainty of 0.5‰ in ε_p. In turn, this will result in a significant error of the pCO_2 estimations, which will be

Table 4. The pCO_2 Estimates Inferred From Diatom Biomarkers From Holocene Arabian Sea Sediments Sampled at Different Sites[a]

Site	SST (°C)	$\delta^{13}C$ (‰)	δ_d (‰)	Biomarker	$\delta^{13}C$ (‰)	ε_p (‰)	b (kg μmol^{-1} L)	$[CO_{2aq}]$ (μmol kg^{-1})	pCO_2 (ppmv)
451	25	2	−8	$C_{25:0}$ HBI	−23.3	9.5	140	9.0	310
453	25	2	−8	$C_{25:0}$ HBI	−21.7	7.8	140	8.1	280
921	25	2	−8	$C_{25:3}$ HBI	−19.9	6.0	140	7.3	250
921	25	2	−8	$C_{25:3}$ HBI	−19.4	5.5	140	7.2	250
921	25	2	−8	$C_{25:4}$ HBI	−21.7	7.8	140	8.1	280

[a]From Netherlands Indian Ocean Program; see *Schouten et al.* [2000].

higher with higher ε_p values. The error caused by uncertainties in SST estimates is twofold. An increase of 1°C causes ε_p to increase with ~0.12‰. The second uncertainty is in the sensitivity of the Arctic SST on the pCO_2 estimates as the solubility of CO_2 is higher under lower seawater temperatures. In comparison with uncertainties in $\delta^{13}C_{pf}$, an uncertainty in SST does not result in a large error in the pCO_2 estimates (10–100 ppmv per 1°C) and depends on the amount of $[CO_2]_{aq}$. Thus, uncertainties in SST cause a relatively minor effect on our pCO_2 estimates. Nevertheless, our 'background'-ETM2 pCO_2 estimates are in agreement with other estimates using proxy data [*Demicco et al.*, 2003; *Lowenstein and Demicco*, 2006] and modeling [*Berner and Kothavala*, 2001; *Pagani et al.*, 2006a; *Zeebe et al.*, 2009] for the early/middle Eocene.

[33] Clearly, further research constraining the viability of this approach is needed. Especially, a good calibration between biomarker $\delta^{13}C$, ε_p and pCO_2 based on modern microorganisms other than haptophytes, is essential to gain better insight in the factors that influence isotopic fractionation as discussed in the previous section. These calibrations are needed to test the assumptions that are at the base of our pCO_2 reconstructions. Another way to test the reliability of our fractionation model is to compare estimated pCO_2 using existing $\delta^{13}C$ records of organic biomarkers with better-constrained pCO_2 conditions during past intervals, such as the last glacial cycles. As a first step, we used the $\delta^{13}C$ of biomarkers of C_{25} HBIs in Holocene sediments of the Arabian Sea [*Schouten et al.*, 2000] to estimate preindustrial pCO_2 levels using our method. We arrive at values between 250 to 300 ppmv, which compares favorably well with preindustrial pCO_2 values (Table 4).

5. Conclusions

[34] We measured concentrations and the $\delta^{13}C$ composition of sulfur-bound biomarkers of marine algal and bacterial origin in sediments deposited in the Arctic Ocean during ETM2, which record environmental change and primary producer responses. Prior to ETM2, the depositional environment was eutrophic with anoxic bottom water conditions, evident from the high TOC content and the presence of sulfur-bound chemical fossils. The various biomarkers show a negative CIE of 3–4.5‰, synchronously with a CIE of 3.5‰ in $\delta^{13}C_{TOC}$, confirming a decrease in the $\delta^{13}C$ of the global exogenic carbon pool. Biomarker concentrations and carbon isotope records indicate that primary productivity increased during ETM2. This led to higher oxygen consumption and contributed to the development of photic zone euxinia. The CIE of the biomarkers is larger than that recorded in marine carbonates, suggesting an increase in the isotopic fractionation of the marine primary producers, likely due to elevated pCO_2 levels. Using the carbon isotopic fractionation factors, we made a first attempt to reconstruct atmospheric CO_2 concentrations and yield a potential range in pCO_2 values of 800 to 1100 ppmv (3 to 4 × preindustrial values) and 1100 to >2000 ppmv (4 to >7 × preindustrial values) for the preexcursion and ETM2, respectively. However, these estimations are subjected to large limiting factors and uncertainties. Critically, to estimate carbon isotopic fractionation factors we adopted the surface water $\delta^{13}C$ DIC values of Walvis Ridge as a representative of the Arctic Ocean surface waters during ETM2. In addition, our pCO_2 estimates are based on the assumption that the ε_p-$[CO_{2aq}]$ relationship, originally calibrated for the $\delta^{13}C$ composition of alkenones, is also applicable for other biomarkers. Therefore, our estimated pCO_2 values should be considered with care. Rather, they are meant to give an idea on what scale pCO_2 levels may have changed during an Eocene hyperthermal. A more thorough testing of the use of $\delta^{13}C$ composition of biomarkers derived from marine microorganisms for $pCO2$ reconstructions is needed, before this method can be used as a tool for reconstructing pCO_2 conditions of past climate.

[35] **Acknowledgments.** This research used samples and data provided by the Integrated Ocean Drilling Program (IODP). This is publication number DW-2011-1007 of the Darwin Center for Biogeosciences, which partially funded this project. A.S. thanks the Netherlands Organization for Scientific Research (NWO) for funding (Veni grant 863.07.001) and the European Research Council under the European Community's Seventh Framework Program for ERC Starting Grant 259627. We thank Jerry Dickens, Mark Pagani, and two anonymous reviewers for their critical comments on the manuscript and M. Kienhuis, J. Ossebaar, and A. Mets for their technical support.

References

Andersen, N., P. J. Müller, G. Kirst, and R. R. Schneider (1999), Alkenone $\delta^{13}C$ as a proxy for past PCO_2 in surface waters: Results from the Late Quaternary Angola Current, in *Use of Proxies in Paleoceanography: Examples from the South Atlantic*, edited by G. Fischer and G. Wefer, pp. 469–488, Springer, Berlin.

Benthien, A., N. Andersen, P. J. Müller, R. R. Schneider, and G. Wefer (1999), Alkenone $\delta^{13}C$-derived pCO_2 levels in surface waters of the southern Atlantic: Holocene vs. last Glacial maximum, paper presented at ASLO Aquatic Science Meeting, Am. Soc. of Limnol. and Oceaogr., Santa Fe, N. M., 1–5 Feb.

Benthien, A., N. Andersen, S. Schulte, P. J. Müller, R. R. Schneider, and G. Wefer (2002), Carbon isotopic composition of the $C_{37:2}$ alkenone in core top sediments of the South Atlantic Ocean: Effects of CO_2 and nutrient concentrations, *Global Biogeochem. Cycles*, *16*(1), 1012, doi:10.1029/2001GB001433.

Berner, R. A. (2006), GEOCARBSULF: A combined model for Phanerozoic atmospheric O_2 and CO_2, *Geochim. Cosmochim. Acta*, *70*, 5653–5664, doi:10.1016/j.gca.2005.11.032.

Berner, R. A., and Z. Kothavala (2001), GEOCARB III: A revised model of atmospheric CO_2 over phanerozoic time, *Am. J. Sci.*, *301*, 182–204, doi:10.2475/ajs.301.2.182.

Bice, K. L., D. Birgel, P. A. Meyers, K. A. Dahl, K.-U. Hinrichs, and R. D. Norris (2006), A multiple proxy and model study of Cretaceous upper

ocean temperatures and atmospheric CO_2 concentrations, *Paleoceanography*, *21*, PA2002, doi:10.1029/2005PA001203.

Bidigare, R. R., et al. (1997), Consistent fractionation of ^{13}C in nature and in the laboratory: Growth-rate effects in some haptophyte algae, *Global Biogeochem. Cycles*, *11*, 279–292, doi:10.1029/96GB03939.

Bijl, P. K., A. J. P. Houben, S. Schouten, S. M. Bohaty, A. Sluijs, G.-J. Reichart, J. S. Sinninghe Damsté, and H. Brinkhuis (2010), Transient Middle Eocene atmospheric CO_2 and temperature variations, *Science*, *330*, 819–821, doi:10.1126/science.1193654.

Bowen, G. J., P. K. Koch, P. D. Gingerich, R. D. Norris, S. Bains, and R. M. Corfield (2001), Refined isotope stratigraphy across the continental Paleocene-Eocene boundary on Polecat Bench in the Northern Bighorn Basin, in *Paleocene-Eocene Stratigraphy and Biotic Change in the Bighorn and Clarks Fork Basins, Wyoming*, *Pap. Paleontol.*, vol. 33, edited by P. D. Gingerich, pp. 73–88, Univ. of Mich., Ann Arbor.

Bowen, G. J., D. J. Beerling, P. L. Koch, J. C. Zachos, and T. Quattlebaum (2004), A humid climate state during the Palaeocene/Eocene thermal maximum, *Nature*, *432*, 495–499, doi:10.1038/nature03115.

Brassell, S. C., C. A. Lewis, J. W. de Leeuw, F. de Lange, and J. S. Sinninghe Damsté (1986), Isoprenoid thiophenes: Novel products of sediment diagenesis?, *Nature*, *320*, 160–162, doi:10.1038/320160a0.

Burkhardt, S., U. Riebesell, and I. Zondervan (1999), Effects of growth rate, CO_2 concentration, and cell size on the stable carbon isotope fractionation in marine phytoplankton, *Geochim. Cosmochim. Acta*, *63*, 3729–3741, doi:10.1016/S0016-7037(99)00217-3.

Cassar, N., E. A. Laws, and B. N. Popp (2006), Carbon isotopic fractionation by the mairne diatom *Phaeodactylum tricornutum* under nutrient- and light-limited growth conditions, *Geochim. Cosmochim. Acta*, *70*, 5323–5335, doi:10.1016/j.gca.2006.08.024.

Cramer, B. S., J. D. Wright, D. V. Kent, and M.-P. Aubry (2003), Orbital climate forcing of $\delta^{13}C$ excursions in the late Paleocene-early Eocene (chrons C24n–C25n), *Paleoceanography*, *18*(4), 1097, doi:10.1029/2003PA000909.

Demicco, R. V., T. K. Lowenstein, and L. A. Hardie (2003), Atmospheric pCO_2 since 60 Ma from records of seawater pH, calcium and primary carbonate mineralogy, *Geology*, *31*, 793–796, doi:10.1130/G19727.1.

Dickens, G. R. (2003), Rethinking the global carbon cycle with a large, dynamic and microbially mediated gas hydrate capacitor, *Earth Planet. Sci. Lett.*, *213*, 169–183, doi:10.1016/S0012-821X(03)00325-X.

Dickens, G. R. (2011), Methane release from gas hydrate systems during the Paleocene-Eocene thermal maximum and other past hyperthermal events: Setting appropriate parameters for discussion, *Clim. Past Discuss.*, *7*, 1139–1174, doi:10.5194/cpd-7-1139-2011.

Fischer, W. W., R. E. Summons, and A. Pearson (2005), Targeted genomic detection of biosynthetic pathways: Anaerobic production of hopanoid biomarkers by a common sedimentary microbe, *Geobiology*, *3*, 33–40, doi:10.1111/j.1472-4669.2005.00041.x.

Freeman, K. H., and J. M. Hayes (1992), Fractionation of carbon isotopes by phytoplankton and estimates of ancient CO_2 levels, *Global Biogeochem. Cycles*, *6*, 185–198, doi:10.1029/92GB00190.

Giordano, M., J. Beardall, and J. A. Raven (2005), CO_2 concentrating mechanisms in algae: mechanisms, environmental modulation, and evolution, *Annu. Rev. Plant Biol.*, *56*, 99–131, doi:10.1146/annurev.arplant.56.032604.144052.

Goericke, R., J. P. Montoya, and B. Fry (1994), Physiology of isotopic fractionation in algae and cyanobacteria, in *Stable Isotopes in Ecology and Environmental Science*, edited by K. Lajtha and R. Michener, pp. 187–221, Blackwell Sci., London.

Greenwood, D. R., and S. L. Wing (1995), Eocene continental climates and latitudinal temperature gradients, *Geology*, *23*, 1044–1048, doi:10.1130/0091-7613(1995)023<1044:ECCALT>2.3.CO;2.

Handley, L., P. N. Pearson, I. K. McMillan, and R. D. Pancost (2008), Large terrestrial and marine carbon and hydrogen isotope excursions in a new Paleocene/Eocene boundary section from Tanzania, *Earth Planet. Sci. Lett.*, *275*, 17–25, doi:10.1016/j.epsl.2008.07.030.

Hayes, J. M. (1999), The abundance of ^{13}C in marine organic matter and isotopic fractionation in the global biogeochemical cycle of carbon during the past 800 Ma, *Chem. Geol.*, *161*, 103–125, doi:10.1016/S0009-2541(99)00083-2.

Hayes, J. M. (2001), Fractionation of the isotopes of carbon and hydrogen in biosynthetic processes, in *Stable Isotope Geochemistry*, *Rev. Mineral. Geochem.*, vol. 43, edited by J. W. Valley and D. Cole, pp. 225–278, Mineral. Soc.of Am., Washington, D. C.

Jaramillo, C., et al. (2010), Effects of rapid global warming at the Paleocene-Eocene boundary on neotropical vegetation, *Science*, *330*, 957–961, doi:10.1126/science.1193833.

Jarvis, I., J. S. Lignum, D. R. Gröcke, H. C. Jenkyns, and M. A. Pearce (2011), Black shale deposition, atmospheric CO_2 drawdown, and cooling during the Cenomanian-Turonian Oceanic Anoxic Event, *Paleoceanography*, *26*, PA3201, doi:10.1029/2010PA002081.

Jasper, J. P., and J. M. Hayes (1990), A carbon isotope record of CO_2 levels during the late Quaternary, *Nature*, *347*, 462–464, doi:10.1038/347462a0.

John, C. M., S. M. Bohaty, J. C. Zachos, A. Sluijs, S. Gibbs, H. Brinkhuis, and T. J. Bralower (2008), North American continental margin records of the Paleocene-Eocene thermal maximum: Implications for global carbon and hydrological setting, *Paleoceanography*, *23*, PA2217, doi:10.1029/2007PA001465.

Kennett, J. P., and L. D. Stott (1991), Abrupt deep-sea warming, palaeoceanographic changes and benthic extinctions at the end of the Palaeocene, *Nature*, *353*, 225–229, doi:10.1038/353225a0.

Knies, J., U. Mann, B. N. Popp, R. Stein, and H.-J. Brumsack (2008), Surface water productivity and paleoceanographic implications in the Cenozoic Arctic Ocean, *Paleoceanography*, *23*, PA1S16, doi:10.1029/2007PA001455.

Kohnen, M. E. L., J. S. Sinninghe Damsté, J. Rullkötter, H. L. ten Haven, and J. W. de Leeuw (1990), Origin and diagenetic transformations of C_{25} and C_{30} highly branched isoprenoid sulfur-compounds: Further evidence for the formation of organically bound sulfur during early diagenesis, *Geochim. Cosmochim. Acta*, *54*, 3053–3063, doi:10.1016/0016-7037(90)90121-Z.

Kohnen, M. E. L., J. S. Sinninghe Damsté, and J. W. de Leeuw (1991), Biases from natural sulphurization in palaeoenvironmental reconstruction based on hydrocarbon biomarker distributions, *Nature*, *349*, 775–778, doi:10.1038/349775a0.

Kohnen, M. E. L., S. Schouten, J. S. Sinninghe Damsté, J. W. de Leeuw, D. A. Merritt, and J. M. Hayes (1992), Recognition of paleobiochemicals by a combined molecular sulfur and isotope geochemical approach, *Science*, *256*, 358–362, doi:10.1126/science.256.5055.358.

Koopmans, M. P., J. Köster, H. M. E. van Kaam-Peters, F. Kenig, S. Schouten, W. A. Hartgers, J. W. de Leeuw, and J. S. Sinninghe Damsté (1996), Diagenetic and catagenetic products of isorenieratene: Molecular indicators for photic zone anoxia, *Geochim. Cosmochim. Acta*, *60*, 4467–4496, doi:10.1016/S0016-7037(96)00238-4.

Koopmans, M. P., W. I. C. Rijpstra, M. M. Klapwijk, J. W. de Leeuw, M. D. Lewan, and J. S. Sinninghe Damsté (1999), A thermal and chemical degradation approach to decipher pristane and phytane precursors in sedimentary organic matter, *Org. Geochem.*, *30*, 1089–1104, doi:10.1016/S0146-6380(99)00088-1.

Laws, E. A., B. N. Popp, R. Bidigare, M. C. Kennicutt, and S. A. Macko (1995), Dependence of phytoplankton carbon isotopic composition on growth rate and $[CO_2]_{aq.}$: Theoretical considerations and experimental results, *Geochim. Cosmochim. Acta*, *59*, 1131–1138, doi:10.1016/0016-7037(95)00030-4.

Leon-Rodriguez, L., and G. R. Dickens (2010), Constraints on ocean acidification associated with rapid an massive carbon injections: The early Paleogene record at ocean drilling program site 1215, equatorial Pacific Ocean, *Palaeogeogr. Palaeoclimatol. Palaeoecol.*, *298*, 409–420, doi:10.1016/j.palaeo.2010.10.029.

Lourens, L. J., A. Sluijs, D. Kroon, J. C. Zachos, E. Thomas, U. Röhl, J. Bowles, and I. Raffi (2005), Astronomical pacing of late Palaeocene to early Eocene global warming events, *Nature*, *435*, 1083–1087, doi:10.1038/nature03814.

Lowenstein, T. K., and R. V. Demicco (2006), Elevated Eocene atmospheric CO_2 and its subsequent decline, *Science*, *313*, 1928–1929, doi:10.1126/science.1129555.

Massé, G., S. T. Belt, S. J. Rowland, and M. Rohmer (2004), Isoprenoid biosynthesis in the diatoms *Rhizosolenia setigera* (Brightwell) and *Haslea ostrearia* (Simonsen), *Proc. Natl. Acad. Sci. U. S. A.*, *101*, 4413–4418, doi:10.1073/pnas.0400902101.

McCarren, H., E. Thomas, T. Hasegawa, U. Röhl, and J. C. Zachos (2008), Depth dependency of the Paleocene-Eocene carbon isotope excursion: Paired benthic and terrestrial biomarker records (Ocean Drilling Program Leg 208, Walvis Ridge), *Geochem. Geophys. Geosyst.*, *9*, Q10008, doi:10.1029/2008GC002116.

Mook, W. G., J. C. Bommerson, and W. H. Staverman (1974), Carbon isotope fractionation between dissolved bicarbonate and gaseous carbon dioxide, *Earth Planet. Sci. Lett.*, *22*, 169–176, doi:10.1016/0012-821X(74)90078-8.

Nicolo, M. J., G. R. Dickens, C. J. Hollis, and J. C. Zachos (2007), Multiple early Eocene hyperthermals: Their sedimentary expression on the New Zealand continental margin and in the deep sea, *Geology*, *35*, 699–702, doi:10.1130/G23648A.1.

Oakes, J. M., A. T. Revill, R. M. Connolly, and S. I. Blackburn (2005), Measuring carbon isotope ratios of microphytobenthos using compound-specific stable isotope analysis of phytol, *Limnol. Oceanogr. Methods*, *3*, 511–519, doi:10.4319/lom.2005.3.511.

Ogawa, Y., K. Takahashi, T. Yamanaka, and J. Onodera (2009), Significance of euxinic condition in the middle Eocene paleo-Arctic basin: A geochemical study on the IODP Arctic Coring Expedition 302 sediments, *Earth Planet. Sci. Lett.*, *285*, 190–197, doi:10.1016/j.epsl.2009.06.011.

O'Regan, M., et al. (2008), Mid-Cenozoic tectonic and paleoenvironmental setting of the central Arctic Ocean, *Paleoceanography*, *23*, PA1S20, doi:10.1029/2007PA001559.

Pagani, M. (2002), The alkenone-CO_2 proxy and ancient atmospheric carbon dioxide, *Philos. Trans. R. Soc. Ser. A*, *360*, 609–632.

Pagani, M., M. A. Arthur, and K. H. Freeman (1999), Miocene evolution of atmospheric carbon dioxide, *Paleoceanography*, *14*, 273–292, doi:10.1029/1999PA900006.

Pagani, M., K. H. Freeman, N. Ohkouchi, and K. Caldeira (2002), Comparison of water column [CO_{2aq}] with sedimentary alkenone-based estimates: A test of the alkenone-CO_2 proxy, *Paleoceanography*, *17*(4), 1069, doi:10.1029/2002PA000756.

Pagani, M., J. C. Zachos, K. H. Freeman, B. Tipple, and S. Bohaty (2005), Marked decline in atmospheric carbon dioxide concentrations during the Paleogene, *Science*, *309*, 600–603, doi:10.1126/science.1110063.

Pagani, M., K. Caldeira, D. Archer, and J. C. Zachos (2006a), An ancient carbon mystery, *Science*, *314*, 1556–1557, doi:10.1126/science.1136110.

Pagani, M., et al. (2006b), Arctic hydrology during global warming at the Palaeocene/Eocene thermal maximum, *Nature*, *442*, 671–675, doi:10.1038/nature05043.

Palmer, M. R., G. J. Brummer, M. J. Cooper, H. Elderfield, M. J. Greaves, G. J. Reichart, S. Schouten, and J. M. Yu (2010), Multi-proxy reconstruction of surface water pCO_2 in the northern Arabian Sea since 29 ka, *Earth Planet. Sci. Lett.*, *295*, 49–57, doi:10.1016/j.epsl.2010.03.023.

Popp, B. N., R. Takigiku, J. M. Hayes, J. W. Louda, and E. W. Baker (1989), The post-Paleozoic chronology and mechanism of 13C depletion in primary marine organic matter, *Am. J. Sci.*, *289*, 436–454.

Popp, B. N., F. Kenig, S. G. Wakeham, E. A. Laws, and R. R. Bidigare (1998a), Does growth rate affect ketone unsaturation and intracellular carbon isotopic variability in *Emiliana huxleyi*?, *Paleoceanography*, *13*, 35–41, doi:10.1029/97PA02594.

Popp, B. N., E. A. Laws, R. R. Bidigare, J. E. Dore, K. L. Hanson, and S. G. Wakeham (1998b), Effect of phytoplankton cell geometry on carbon isotopic fractionation, *Geochim. Cosmochim. Acta*, *62*, 69–77, doi:10.1016/S0016-7037(97)00333-5.

Quandt, L., G. Gottschalk, H. Ziegler, and W. Stichler (1977), Isotope discrimination by photosynthetic bacteria, *FEMS Microbiol. Lett.*, *1*, 125–128, doi:10.1111/j.1574-6968.1977.tb00596.x.

Rau, G. H., U. Riebesell, and D. A. Wolf-Gladrow (1996), A model of photosynthetic ^{13}C fractionation by marine phytoplankton based on diffusive molecular CO_2 uptake, *Mar. Ecol. Prog. Ser.*, *133*, 275–285, doi:10.3354/meps133275.

Rohmer, M., P. Bisseret, and S. Neunlist (1992), The hopanoids, prokaryotic triterpenoids and precursors of ubiquitous molecular fossils, in *Biological Markers in Sediments and Petroleum*, edited by J. M. Moldowan, P. Albercht, and R. P. Philp, pp. 1–17, Prentice Hall, Englewood Cliffs, N. J.

Royer, D. L., C. P. Osborne, and D. J. Beerling (2002), High CO_2 increases the freezing sensitivity of plants: Implications for paleoclimatic reconstructions from fossil floras, *Geology*, *30*, 963–966, doi:10.1130/0091-7613(2002)030<0963:HCITFS>2.0.CO;2.

Sakata, S., J. M. Hayes, A. R. McTaggart, R. A. Evans, K. J. Leckrone, and R. K. Togasaki (1997), Carbon isotopic fractionation associated with lipid biosynthesis by a cyanobacterium: Relevance for interpretation of biomarker records, *Geochim. Cosmochim. Acta*, *61*, 5379–5389, doi:10.1016/S0016-7037(97)00314-1.

Schoell, M., S. Schouten, J. S. Sinninghe Damsté, J. W. de Leeuw, R. E. Summons, and R. E. Summons (1994), A molecular organic carbon isotope record of Miocene climate changes, *Science*, *263*, 1122–1125, doi:10.1126/science.263.5150.1122.

Schouten, S., W. C. M. Klein Breteler, P. Blokker, N. Schogt, W. I. C. Rijpstra, K. Grice, M. Baas, and J. S. Sinninghe Damsté (1998), Biosynthetic effects on the stable carbon isotopic compositions of algal lipids: Implications for deciphering the carbon isotopic biomarker record, *Geochim. Cosmochim. Acta*, *62*, 1397–1406, doi:10.1016/S0016-7037(98)00076-3.

Schouten, S., M. J. L. Hoefs, and J. S. Sinninghe Damsté (2000), A molecular and stable carbon isotopic study of lipids in late Quaternary sediments from the Arabian Sea, *Org. Geochem.*, *31*, 509–521, doi:10.1016/S0146-6380(00)00031-0.

Schouten, S., M. Woltering, W. I. C. Rijpstra, A. Sluijs, H. Brinkhuis, and J. S. Sinninghe Damsté (2007), The Paleocene-Eocene carbon isotope excursion in higher plant organic matter: Differential fractionation of angiosperms and conifers in the Arctic, *Earth Planet. Sci. Lett.*, *258*, 581–592, doi:10.1016/j.epsl.2007.04.024.

Sinninghe Damsté, J. S., and J. W. de Leeuw (1990), Analysis, structure and geochemical significance of organically bound sulphur in the geosphere: State of the art and future research, *Org. Geochem.*, *16*, 1077–1101, doi:10.1016/0146-6380(90)90145-P.

Sinninghe Damsté, J. S., W. I. C. Rijpstra, J. W. de Leeuw, and P. A. Schenk (1988), Origin of organic sulphur compounds and sulphur-containing high molecular weight substances in sediments and immature crude oils, *Org. Geochem.*, *13*, 593–606, doi:10.1016/0146-6380(88)90079-4.

Sinninghe Damsté, J. S., S. G. Wakeham, M. E. L. Kohnen, J. M. Hayes, and J. W. de Leeuw (1993), A 6,000-year sedimentary molecular record of chemocline excursions in the Black Sea, *Nature*, *362*, 827–829, doi:10.1038/362827a0.

Sinninghe Damsté, J. S., et al. (2004a), The rise of the rhizosolenid diatoms, *Science*, *304*, 584–587, doi:10.1126/science.1096806.

Sinninghe Damsté, J. S., W. I. C. Rijpstra, S. Schouten, J. A. Fuerst, M. S. M. Jetten, and M. Strous (2004b), The occurrence of hopanoids in planctomycetes: Implications for the sedimentary biomarker record, *Org. Geochem.*, *35*, 561–566, doi:10.1016/j.orggeochem.2004.01.013.

Sinninghe Damsté, J. S., M. M. M. Kuypers, R. D. Pancost, and S. Schouten (2008), The carbon isotopic response of algae, (cyano) bacteria, archaea and higher plants to the late Cenomanian perturbation of the global carbon cycle: Insights from biomarkers in black shales from the Cape Verde Basin (DSDP Site 367), *Org. Geochem.*, *39*, 1708–1718.

Sluijs, A., J. Pross, and H. Brinkhuis (2005), From greenhouse to icehouse; organic-walled dinoflagellate cysts as paleoenvironmental indicators in the Paleogene, *Earth Sci. Rev.*, *68*, 281–315, doi:10.1016/j.earscirev.2004.06.001.

Sluijs, A., et al. (2006), Subtropical Arctic Ocean temperatures during the Palaeocene/Eocene thermal maximum, *Nature*, *441*, 610–613, doi:10.1038/nature04668.

Sluijs, A., G. J. Bowen, H. Brinkhuis, L. J. Lourens, and E. Thomas (2007), The Palaeocene-Eocene Thermal Maximum super greenhouse: Biotic and geochemical signatures, age models and mechanisms of global change, in *Deep-Time Perspectives on Climate Change: Marrying the Signal From Computer Models and Biological Proxies*, edited by M. Williams et al., pp. 323–349, Geol. Soc., London.

Sluijs, A., U. Röhl, S. Schouten, H.-J. Brumsack, F. Sangiorgi, J. S. Sinninghe Damsté, and H. Brinkhuis (2008), Arctic late Paleocene-early Eocene paleoenvironments with special emphasis on the Paleocene-Eocene thermal maximum (Lomonosov Ridge, Integrated Ocean Drilling Program Expedition 302), *Paleoceanography*, *23*, PA1S11, doi:10.1029/2007PA001495.

Sluijs, A., S. Schouten, T. H. Donders, P. L. Schoon, U. Röhl, G. J. Reichart, F. Sangiorgi, J.-H. Kim, J. S. Sinninghe Damsté, and H. Brinkhuis (2009), Warm and wet conditions in the Arctic region during Eocene Thermal Maximum 2, *Nat. Geosci.*, *2*, 777–780, doi:10.1038/ngeo668.

Smith, F. A., S. L. Wing, and K. H. Freeman (2007), Magnitude of the carbon isotope excursion at the Paleocene-Eocene thermal maximum: The role of plant community change, *Earth Planet. Sci. Lett.*, *262*, 50–65, doi:10.1016/j.epsl.2007.07.021.

Stap, L., A. Sluijs, E. Thomas, and L. Lourens (2009), Patterns and magnitude of deep sea carbonate dissolution during Eocene Thermal Maximum 2 and H2, Walvis Ridge, southeastern Atlantic Ocean, *Paleoceanography*, *24*, PA1211, doi:10.1029/2008PA001655.

Stap, L., L. J. Lourens, E. Thomas, A. Sluijs, S. Bohaty, and J. C. Zachos (2010), High-resolution deep-sea carbon and oxygen isotope records of Eocene Thermal Maximum 2 and H2, *Geology*, *38*, 607–610, doi:10.1130/G30777.1.

Stein, R., B. Boucsein, and H. Meyer (2006), Anoxia and high primary production in the Paleogene central Arctic Ocean: First detailed records from Lomonosov Ridge, *Geophys. Res. Lett.*, *33*, L18606, doi:10.1029/2006GL026776.

Summons, R. E., L. L. Jahnke, J. M. Hope, and G. A. Logan (1999), 2-Methylhopanoids as biomarkers for cyanobacterial oxygenic photosynthesis, *Nature*, *400*, 554–557, doi:10.1038/23005.

Talbot, H. M., R. E. Summons, L. L. Jahnke, C. S. Cockell, M. Rohmer, and P. Farrimond (2008), Cyanobacterial bacteriohopanepolyol signatures from cultures and natural environmental settings, *Org. Geochem.*, *39*, 232–263, doi:10.1016/j.orggeochem.2007.08.006.

Thomas, D. J., J. C. Zachos, T. J. Bralower, and S. Bohaty (2002), Warming the fuel for the fire: Evidence for the thermal dissociation of methane hydrate during the Paleocene-Eocene thermal maximum, *Geology*, *30*, 1067–1070, doi:10.1130/0091-7613(2002)030<1067:WTFFTF>2.0.CO;2.

Tripati, A., and H. Elderfield (2005), Deep-sea temperature and circulation changes at the Paleocene-Eocene thermal maximum, *Science*, *308*, 1894–1898, doi:10.1126/science.1109202.

Uchikawa, J., and R. E. Zeebe (2010), Examining possible effects of seawater pH decline on foraminiferal stable isotopes during the Paleocene-Eocene Thermal Maximum, *Paleoceanography*, *25*, PA2216, doi:10.1029/2009PA001864.

Valisolalao, J., N. Perakis, B. Chappe, and P. Albrecht (1984), A novel sulfur containing C_{35} hopanoid in sediments, *Tetrahedron Lett.*, *25*, 1183–1186, doi:10.1016/S0040-4039(01)91555-2.

Van Breugel, Y., S. Schouten, M. Paetzel, and J. S. Sinninghe Damsté (2006), Seasonal variation in the stable carbon isotopic composition of algal lipids in a shallow anoxic fjord: Evaluation of the effect of recycling of respired CO_2 on the $\delta^{13}C$ of organic matter, *Am. J. Sci.*, *306*, 367–387, doi:10.2475/05.2006.03.

van der Meer, M. T. J., S. Schouten, and J. S. Sinninghe Damsté (1998), The effect of the reversed tricarboxylic acid cycle on the ^{13}C contents of bacterial lipids, *Org. Geochem.*, *28*, 527–533, doi:10.1016/S0146-6380(98)00024-2.

Volkman, J. K., S. M. Barrett, and G. A. Dunstan (1994), C_{25} and C_{30} highly branched isoprenoid alkenes in laboratory cultures of two marine diatoms, *Org. Geochem.*, *21*, 407–414, doi:10.1016/0146-6380(94)90202-X.

Weijers, W. H., S. Schouten, A. Sluijs, H. Brinkhuis, and J. S. Sinninghe Damsté (2007), Warm Arctic continents during the Palaeocene-Eocene thermal maximum, *Earth Planet. Sci. Lett.*, *261*, 230–238, doi:10.1016/j.epsl.2007.06.033.

Weiss, R. F. (1974), Carbon dioxide in water and seawater: The solubility of a non-ideal gas, *Mar. Chem.*, *2*, 203–215, doi:10.1016/0304-4203(74)90015-2.

West, N., R. Alexander, and R. I. Kagi (1990), The use of silicalite for rapid isolation of branched and cyclic alkane fractions of petroleum, *Org. Geochem.*, *15*, 499–501, doi:10.1016/0146-6380(90)90095-H.

Wing, S. L., G. J. Harrington, F. A. Smith, J. I. Bloch, D. M. Boyer, and K. H. Freeman (2005), Transient floral change and rapid global warming at the Paleocene-Eocene boundary, *Science*, *310*, 993–996, doi:10.1126/science.1116913.

Zachos, J. C., G. R. Dickens, and R. E. Zeebe (2008), An early Cenozoic perspective on greenhouse warming and carbon-cycle dynamics, *Nature*, *451*, 279–283, doi:10.1038/nature06588.

Zeebe, R. E., J. C. Zachos, and G. R. Dickens (2009), Carbon dioxide forcing alone insufficient to explain Palaeocene-Eocene Thermal Maximum warming, *Nat. Geosci.*, *2*, 576–580, doi:10.1038/ngeo578.

P. L. Schoon, S. Schouten, and J. S. Sinninghe Damsté, Department of Marine Organic Biogeochemistry, NIOZ Royal Netherlands Institute for Sea Research, PO Box 59, Landsdiep 4, NL-1790 AB Den Burg, Texel, Netherlands. (petra.schoon@nioz.nl)

A. Sluijs, Biomarine Sciences, Laboratory of Palaeobotany and Palynology, Institute of Environmental Biology, Faculty of Science, Utrecht University, Budapestlaan 4, NL-3584 CD Utrecht, Netherlands.